Colloids and Surfaces A 599 (2020) 124824

Contents lists available at ScienceDirect

Colloids and Surfaces A

journal homepage: www.elsevier.com/locate/colsurfa

Green approach of synthesis of thiazolyl imines and their impeding behavior against corrosion of mild steel in acid medium

Ashish Kumar Singh[a,*], Bhawna Chugh[b], Sanjeeve Thakur[b], Balaram Pani[c], Hassane Lgaz[d], Ill-Min Chung[d], Shweta Pal[e], Rajiv Prakash[e]

[a] Department of Applied Sciences, Bharati Vidyapeeth's College of Engineering, New Delhi 110063, India
[b] Department of Chemistry, Netaji Subhas Institute of Technology, University of Delhi, New Delhi 110078,India
[c] Department of Chemistry, Bhaskaracharya College of Applied Science, University of Delhi, New Delhi 110078, India
[d] Department of Crop Science, College of Sanghur Life Science, Konkuk University, Seoul 05029, South Korea
[e] School of Material Science and Technology, Indian Institute of Technology (Banaras Hindu University), Varanasi 221005, India

GRAPHICAL ABSTRACT

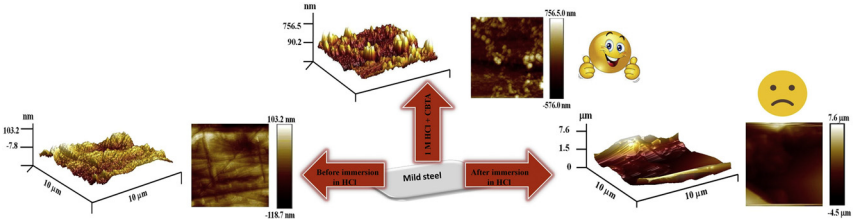

ARTICLE INFO

Keywords:
Ultrasound waves
Corrosion
EIS
XPS
DFT
Monte Carlo

ABSTRACT

Recent advancements regarding synthetic methods of organic molecules, viz. conventional method, and exposure of microwave as well as ultrasound waves led us to synthesize four different thiazolyl imines by different methods like conventional heating and by exposure of ultrasound waves to the mixture of reactants. Ultrasonication was found more efficient, fast and clean method of the synthesis of thiazolyl imines. The synthesized compounds were employed to overcome metallic corrosion problem in various industries, as application of corrosion inhibitor has been a subject of research these days. In view of this, the present work deals with the comprehension of the greener synthetic route for thiazolyl imines and employing those as corrosion inhibitors for investigating acidic corrosion of mild steel using electrochemical, gravimetric, surface and theoretical studies. The thiazolyl imines were found to impede acid corrosion of mild steel (MS) by adsorbing themselves as per Langmuir isotherm. The effect of their adsorption on the surface morphology of MS was studied on micro/nano level using scanning electron microscopy/atomic force microscopy, X-ray spectroscopic studies, viz. energy dispersive X-ray microanalysis (EDXMA) and X-ray photoelectron spectroscopy (XPS), subsequently explaining their adsorption mechanism. The theoretical parameters obtained from computational study of inhibitor molecules explained the experimental findings extremely well.

1. Introduction

The metallic corrosion has been considered as one of the most perilous problem across many industries due to huge economic loss and depletion of our natural resources directly or indirectly. An accurate estimation of annual cost of corrosion is of course impossible but one

* Corresponding author.
E-mail address: ashish.singh.rs.apc@itbhu.ac.in (A.K. Singh).

https://doi.org/10.1016/j.colsurfa.2020.124824
Received 16 January 2020; Received in revised form 20 March 2020; Accepted 2 April 2020
Available online 23 April 2020

can perceive that the cost is enormous if we consider all the cases of corrosion where metals and alloys are used. Recently, corrosion awareness day highlighted the annual corrosion cost to be US$2.5 trillion [1]; reflecting that failure of the policy makers and government in understanding the consequences of corrosion. Thus, in view of this, the protection of assets from corrosion is must. However, that cost can be reduced by $ 875 billion annually through application of highly efficient corrosion diminishing technologies under proper guidance of experienced corrosion professionals [1].

The metals have been proven very important for people since the Bronze Age due to their unique properties viz. mechanical strength and durability. These properties make the metals so useful for people but on the other hand due to their high reactivity, they are prone to corrosion. The high vulnerability of metals to corrosion forced us to think about the use of metallic alloy. The alloying can modify the properties of base metal.

Mild steel is a low carbon alloy of iron. The appreciable mechanical strength and low cost of mild steel make it very important for the manufacturing of metallic items. Because of its beneficial properties, viz. can be cut, bent or twisted easily to take any desired shape, mild steel has been proven very significant material. The low carbon content of mild steel makes it harder but more susceptible to corrosion. Thus, mild steel, in general, cannot be used without protective measures for corrosion.

Metallic corrosion is considered as a major problem for the application of engineering materials in various environments [2]. As a result there is continuous ongoing effort to develop certain protective measures which can effectively protect the materials from corrosion [3]. One such method to control metallic corrosion is the use of inhibitors [4] in corrosive medium to slow down the aggressive attack of corrosive media.

The literature reveals that the presence of hetero atoms, non-bonding electrons and π-electrons make the organic compound an efficient corrosion inhibitor [5,6]. In view of this, thiazole moieties can be considered as a fast growing potential unit in the world of heterocyclic chemistry having very promising characteristics and applications in field of corrosion inhibition. By virtue of this, thiazole derivatives have been reported as effective corrosion inhibitors by many researchers [7–9]. This led us to select some thiazolyl imines with enhanced inhibitory performance to study their anti-corrosive behavior with reference to mild steel corrosion in HCl medium.

Although conventional method of synthesis has mostly been practiced to drive chemical reactions involving multiple reactants to get desired products [10–12], however, application of conventional method to run chemical reactions has encountered number of problems viz.: longer time period for completion of reaction, presence of by-products along with desired one and consumption of considerable amount of energy. These shortcomings can be resolved by the application of more efficient approaches viz. microwave irradiation and exposure of ultrasonic waves [13,14]. The application of these alternative sources of energy offer a realistic option for industry as they provide fast as well as efficient conversion of reactants in to product with maximum possible yield and accompanied with less labor.

However, the use of microwave and ultrasonic waves have been proven excellent option for conventional heat sources to complete chemical reactions more efficiently, nevertheless, the possibility of spot heating associated with microwave assisted method led us to go with ultrasonic wave assisted synthesis of the investigated compounds.

Considering the ecological aspect, research nowadays is drifting towards the progress of using green and sustainable corrosion inhibitors [15,16]. In view of all these facts, this paper presents design of some efficient corrosion inhibitors (thiazolyl imines) on the basis of theoretical parameters (obtained from density functional theory; DFT), their ultrasound waves assisted synthesis and study their corrosion impeding behavior in context to mild steel in HCl medium using gravimetric and electrochemical studies.

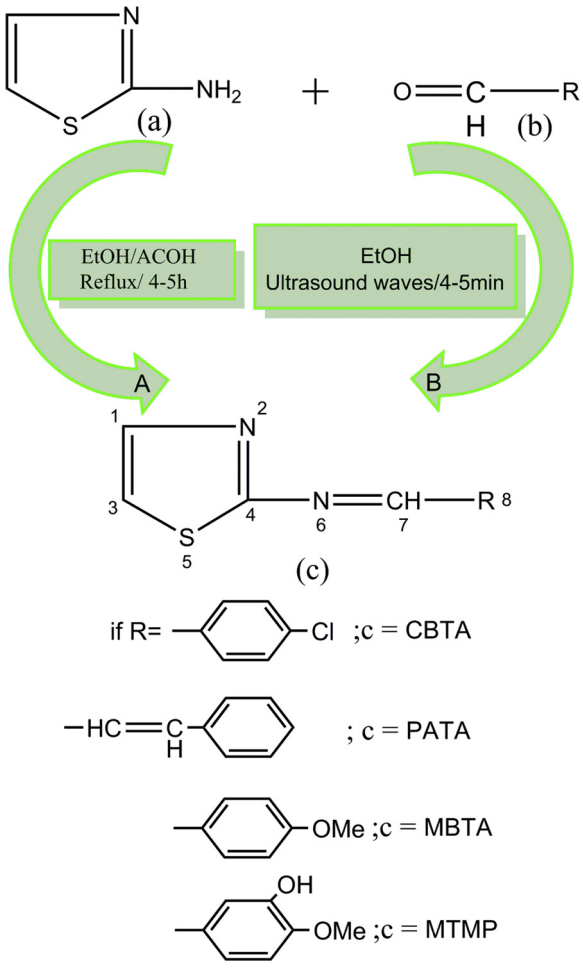

Fig. 1. Scheme of synthesis of the investigated compounds.

2. Experimental procedure & measurements

2.1. Synthesis of thiazolyl imines

The thiazolyl imines were synthesized by both conventional as well as ultrasound wave assisted method. The ultrasound wave assisted synthesis was found fast, clean and offered more efficient production of the thiazolyl imines. In both methods, thiazole-2-amine and different aldehyde were either refluxed in ethanolic solution or exposed to ultrasound waves as per scheme presented in Fig. 1 and resulted in to the production of different thiazolyl imines. The resultant products were filtered, recrystallized and dried. The FT-IR spectra were scanned by Thermo Fisher FTIR spectrometer to confirm the formation of desired compounds. Fig. 2 presents Fourier-transform infrared spectra of synthesized thiazolyl imines and the spectral data obtained are tabulated as Table 1. The elemental analysis of investigated compounds was done by CHN analysis whose data are also given in Table 1. The ^{1}H NMR spectral data of all the synthesized compounds is also presented in Table 1.

2.2. Materials & solutions

Mild steel (MS) having composition 99.7155 Fe, Cr (0.001), C (0.05), 0.20 % Mn, 0.009 % Si, 0.012% P, and 0.0025% Ni by weight were cut in to small coupons of 2.5 × 2.0cm^2 dimension and polished with emery paper of varying grade (200–1200). These MS coupons were used to carry out gravimetric experiments as per standard method [17]. The data of gravimetric experiments were used to calculate surface fraction covered by inhibitor (θ), corrosion impeding efficiency

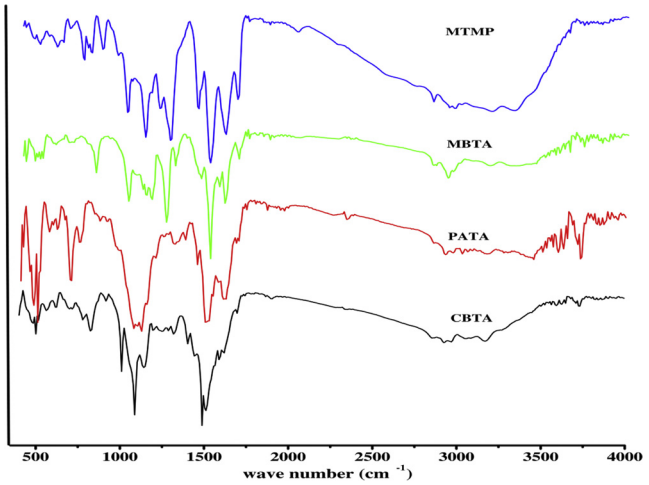

Fig. 2. FT-IR spectra of the synthesized compounds.

(E_{WL} %), and corrosion rate (C_R) as per Eqs. (1), (2) & (3) as [18,19]:

$$\frac{w_0 - w_i}{w_0} = \theta \tag{1}$$

$$\frac{w_0 - w_i}{w_0} \times 100 = \theta \times 100 = E_{WL} \tag{2}$$

$$\frac{87600w}{AtD} = C_R \tag{3}$$

where, w_0, w_i, A, t and D symbolize for mass loss in aggressive solution without thiazolyl imines, mass loss in aggressive solution + thiazolyl imines, A for surface area of metal, t for time of immersion in aggressive solution and D, the density of MS sample respectively.

The aggressive electrolytic acid solution (1 M HCl) was made using 37% HCl supplied from Merck, India. Different thiazolyl imines were added to aggressive solution (1 M HCl) to prepare their stock solution to use further to run the different experiments.

2.3. Electrochemical studies

To run electrochemical experiments, the MS coupons having dimension 7.5 × 1 cm^2 with 1 cm^2 exposed surface area were used for both potentiodynamic scan and EIS studies. All the electrochemical experiments were run on CHI-760 potentiostat. The CHI-760 potentiostat fitted to a triple electrode set; working-MS, counter-Pt, and reference electrode-saturated calomel. The triple electrodes were kept in thermostat to maintain uniform temperature around 308 K during experiments. The MS electrode (working) immersed in different aggressive solutions was kept static for ½ h to stabilize the Open circuit voltage (OCP).The frequency range selected to run impedance experiment (EIS) was 100 kHz to 0.01 Hz. The EIS parameters are deduced from obtained experimental data with the help of CHI 760c software as [20]:

$$\frac{R_p^i - R_p^0}{R_p^i} \times 100 = E_{EIS}\% \tag{4}$$

Where, polarization resistance of mild steel is symbolized by R_p while superscripts i and 0 are written to indicate presence and absence of inhibitor in aggressive solution respectively.

The potential range selected to run PDP was -250 to +250 mV with 0.1 mV sec^{-1} scan rate. All the potentiodynamic parameters were computed from the data obtained. The comparative performance of investigated thiazolyl imines can also be obtained from corrosion current density values obtained from PDP experiments as [21]:

Table 1
Yield, physical and spectral data of the synthesized inhibitors.

Name of Inhibitor	Time taken in synthesis (Min.)		Yield (%)		M.P. (°C)	IR ν (cm^{-1})	^{1}H NMR δ (ppm)	CHN (%)
	Con.	US	Con.	US				
CBTA	210	3.0	78	89	142	501 (C-S-C str), 1488 (C = C), 1504 (C = N str; thiazole), 1638 (HC = N, azomethine), 2923 (Ar-H stretch)	8.48 (s, 1H, N = CH), 7.77 (d, 2H, Ar-H), 7.52 (d, 2H, Ar-H), 7.60(d, 1H, thiazole), 7.87(d, 1H, thiazole)	C = 53.9, H = 3.15, N = 12.6
PATA	240	3.5	76	88	136	694 (C-S-C stretch), 1319 (C = C), 1511 (C = N stretch; Thiazole), 1619 (HC = N, azomethine), 2931 (Ar-H stretch)	7.50(s, 1H, N = CH), 7.60(d, 1H, thiazole), 7.82(d, 1H, thiazole), 5.67(dd, 1H, CH = C), 6.90 (d, 1H, C = CH), 7.60(d, 2H, Ar-H),7.40 (t, 2H, Ar-H), 7.33(t, 1H, Ar-H)	C = 67.3, H = 4.7, N = 13.1
MBTA	270	4.0	75	86	148	586 (C-S-C stretch), 1457 (C = C), 1512 (C = N stretch, Thiazole), 1605 (HC = N, Azomethine), 2931 (Ar-H stretch)	8.28(s, 1H, N = CH). 3.83(s, 3H, methyl), 7.84(d, 2H, Ar-H), 7.06 (d, 2H, Ar-H), 7.84(d, 1H, thiazole), 7.58(d, 1H, thiazole)	C = 60.5, H = 4.61, N = 12.81
MTMP	300	4.0	73	86	152	763 (C-S-C stretch), 1442(C = C), 1511 (C = N stretch, Thiazole), 1604 (HC = N, Azomethine), 2969(Ar-H stretch), 3340 (-OH Stretch)	8.18(s, 1H, N = CH), 3.83(s, 3H, methyl), 5.35(s, 1H, -OH), 6.89(d, 1H, Ar-H), 7.35(d, 1H,Ar-H),7.40(d, 1H, Ar-H), 7.58(d, 1H, thiazole),7.80(d, 1H, thiazole)	C = 56.4, H = 4.31, N = 11.97

$$\frac{i^0_{corr} - i^i_{corr}}{i^0_{corr}} \times 100 = E_{PDP}\% \quad (5)$$

where, i^0_{corr} and i^i_{corr} are written for corrosion current density when MS electrode immersed in mere acid and thiazolyl imines containing acid solutions respectively.

2.4. Surface analysis of working electrode

The exposure of metal surface to aggressive environment causes various morphological changes over the metal surface due its corrosion. Thus, in order to analyze any morphological change, identification of any contaminants over the working electrode, elemental deposition on the working electrode metallic surface, different surface characterization techniques were applied.

2.4.1. Scanning electron microscopy-energy dispersive X-ray microanalysis (SEM-EDXMA)

The morphological change in working electrode caused due to attack of aggressive species present in electrolytic solution can be observed by scanning its surface by SEM. The contamination or elemental deposition over working electrode MS surface can be distinguished by energy dispersive X-ray microanalysis. The morphological analysis was performed by SEM supplied by Hitachi (Hitachi TM 3000) while element detection over working electrode surface was through energy dispersive X-ray microanalysis supplied from OXFORD INSTRUMENTS (SWIFT ED 3000). This analysis was carried out at the supply of 15 kV voltages.

2.4.2. AFM

Use of atomic force microscopy (AFM) eases the analysis of surface topography, as well as local surface roughness measurements. The film developed over working electrode surface is closely related to its protecting efficiency of the metallic substrate against aggressive environment causing corrosion. The application of AFM makes easy the detection of nature of this film.

Atomic force microscopy has been used as a powerful and informative technique to analyze surface morphology from at micro to nano level. Thus, it has become one of the most obvious choices to examine the influence of additives on corrosion at MS/aggressive solution interface.

To scan AFM images of working electrode surface, MS samples were prepared in such a way that they dipped in different aggressive solutions with that concentration of thiazolyl imines which showed maximum corrosion protecting ability for 6 h, carried off and then dried. These MS samples were then ready to capture AFM images. The atomic force microscope used to capture AFM images was supplied from Bruker and the AFM images were captured by running the microscope in tapping mode. The obtained atomic force micrographs were then analyzed by using Nanoscope 8.5 analysis software.

2.4.3. XPS

Study about the relation of property with the surface composition of metallic structure provides basic idea to understand the nature of corrosion. Though conventional corrosion evaluating techniques have been practiced, X-ray photoelectron spectroscopy (XPS) has come out as a powerful and promising tool to analyze the nano level corrosion film developed over the MS surface. The composition of film developed over the surface can be studied by scanning mild steel coupon using Multiprobe surface analysis instrument (Scienta Omicron, Germany). The pressure applied during this scanning was 5×10^{-11}Torr. MS samples was prepared by allowing immersing in acidic solution of MTMP (6 mg L^{-1}) for 6 h, carried off, washed and dried finally. This MS sample was then used to scan XPS spectra.

2.5. Computational analysis

2.5.1. Quantum chemical investigation

DMol [3] of Materials Studio Software provided us all the quantum chemical parameters and Fukui functions [22,23]. Perdew, Burke, and Ernzerhof (PBE) [24] put forwarded generalized gradient approximation (GGA) method of DFT which enabled us to get the optimized geometry of the molecule as well as calculation of Fukui functions by using COSMO implicit solvent [25]. The parameters of chemical reactivity (ionization potential, I and electron affinity, A which measures the electron donating and accepting power of the molecule respectively) of any molecule can be calculated as per Koopmans' as [26]:

$$I,\ i.\ e.\ \text{ionization potential} = -E_{HOMO} \quad (6)$$

$$A,\ \ i.\ e.\ \text{electron affinity} = -E_{LUMO} \quad (7)$$

where, E_{HOMO} represents energy of uppermost occupied and E_{LUMO} signifies energy of vacant orbital lying at lowest level. Further, electronegativity (χ) and absolute hardness (η) can be obtained from the values of I (ionization potential) and A using Eqs. (8) and (9):

$$\chi,\ i.\ e.\ \text{electronegativity} = \frac{I + A}{2} \quad (8)$$

$$\frac{I - A}{2} = \text{absolute hardness},\ \eta \quad (9)$$

The extent of electrons transferred (ΔN) can be obtained as per eqn. (10) as [27]:

$$\frac{1}{\Delta N} = \frac{(\eta_{Fe} + \eta_{inh})}{\phi - \chi_{inh}} \quad (10)$$

The value of ϕ (work function) is generally taken as 4.82 eV for Fe (110) while almost equal value of I and A for bulk metal leads to the value of $\eta_{Fe} = 0$ [28,29].

Fukui functions which measure electrophilic and nucleophilic tendency of molecule can be predicted by introducing finite difference approximations as per Yang and Mortier [30]. Morell et al. [31] projected dual descriptor as a best informative tool to confirm active centers for both nucleophilic (Nu^-C) and electrophilic (E^+C) attack. Hirschfeld Population Analysis (HPA) provided the estimation of these functions as [32]:

For Nu^- attack

$$fu^+_A = -q_A(N) + q_A(N^+) \quad (11)$$

E^+ attack

$$fu^-_A = -q_A(N^-) + q_A(N) \quad (12)$$

And difference of these two functions (Dual descriptor),

$$fu^+_A - fu^-_A = \Delta fu_{(A)} \quad (13)$$

Where, q_A represents a particular atomic site population in its all the three possible states, i.e. cationic (N^+), anionic (N^-), and neutral form (N).

2.5.2. Molecular motion simulations (MMS)

Material studio software was used to accomplish MMS in its Forcite module [22]. An appreciably high stabilizing energy together with extremely packed crystal lattice structure of Fe (110) [33] lead us to choose it as substrate layer. This iron substrate layer along with solvent layer which consists of water, hydronium ion and chlorine is considered in a single simulation case of size 24.82 × 24.82 × 35.69 Å [3]. The process optimization was done by steepest descent accompanied with conjugated grade algorithms [34]. All the simulations were completed by using COMPASS force field [35] and a statistical ensemble involving mechanical (number, N), volume (V) and temperature variable (T).This simulation study is done at 303 K temperature with 2000 ps simulation time and 1 fs time step for completion. The whole simulation is

controlled by Andersen algorithm [36]. At equilibrium, the relation between binding and interaction energy can be written [37] as:

$$E_{total} - (E_{MS\text{-}surface + aggressive\ solution} + E_{additive}) = E_{interaction} \quad (14)$$

In the above equation, $E_{MS\text{-}surface+aggressive\ solution}$, $E_{additive}$, and E_{total} symbolize the energy of the Fe (110)-aggressive solution system devoid of additive, energy of an additive, and total energy of entire system respectively.

3. Results & discussion

3.1. Synthesis & spectral identification

The inhibitors were synthesized by refluxing 2-amino thiazole with different aromatic aldehydes in ethanolic medium in presence of catalytic amount of acetic acid as per scheme presented in Fig. 1. The same sets of compounds were also synthesized by giving exposure of ultrasound waves to an ethanolic mixture of 2-amino thiazole and different aromatic aldehydes. The inhibitors were obtained in appreciable yield. The spectral and elemental analysis data (CHN) confirmed the formation of the thiazolyl imines. The physical and spectral data of the inhibitors are presented as Table 1 and corresponding images are given as Fig. 2a-b.

3.2. Gravimetric study

3.2.1. Relation between additive's amount and corrosion rate

In order to establish an effect of additive's amount on corrosion rate, gravimetric experiments were done in aggressive solution with variable amount of the additives separately. All the gravimetric experiments were repeated thrice and average data were reported as Table 2. The effect of increasing additive's amount of inhibitors is presented as Fig. 3. The experimental results noticed that attack of aggressive solution lessened by the increasing additive's amount. This is because of the fact that with increasing concentration of inhibitor, adsorption capacity increases leaving behind less available sites for the adsorption of corrosion causing species (H_2O, Cl^-). This represents initial predominantly electrostatic adsorption of additive molecule replacing aggressive attacking species from the MS surface.

3.2.2. Comparative effectiveness of thiazolyl imines

Performance of the thiazolyl imines against attack of aggressive solution to metal surface was further compared with some similar organic molecules which were earlier studied [38–41]. The comparative performance of the inhibitors is presented in Table 3 which shows that the corrosion impeding potential of thiazolyl imines, CBTA, PATA, MBTA, and MTMP is either superior or comparable to other earlier studied inhibitors even at much low concentration. The presence of electron donor groups, $-OH$ and $-OCH_3$ probably make MTMP pre-eminent performer than others.

3.2.3. Influence of inhibitor on corrosion kinetics

Valuable information regarding effect of additives on the kinetics aspect of corrosion can be drawn by determining activation parameters. Gravimetric experimentations were made at four different sets of temperatures with variable amount of additives to draw information about kinetic parameters. The linearity of log C_R and log C_R/T vs. $1/T$ for different aggressive solutions confirmed that the kinetics of corrosion and its inhibition both follow Arrhenius and transition state equation. According to Arrhenius and transition state equation [42]

$$\log C_R = \frac{-E_a}{2.303RT} + \log\lambda \quad (15)$$

$$C_R = \frac{RT}{Nh}\exp\left(\frac{\Delta S^*}{R}\right)\exp\left(\frac{-\Delta H^*}{RT}\right) \quad (16)$$

Where, C_R, E_a, λ, ΔS^* and ΔH^* stand for corrosion rate, free energy of activation, Arrhenius pre-exponential factor, activation entropy and enthalpy respectively. All other symbols have their usual meaning.

Fig. 4 presents graphs obtained by plotting log C_R vs. $1/T$ obtained from gravimetric experimentations performed at four different sets of temperatures in different aggressive solutions. The linearity ($R^2 \approx 1$) of all the straight lines confirms the kinetic control of processes, corrosion and its inhibition.

The values of E_a and λ deduced for different amount of thiazolyl imines, CBTA, PATA, MBTA and, MTMP are specified in Table 4. The values of E_a are higher for inhibited solutions with different inhibitors, i.e. 38.28-44.3 kJ mol^{-1} for CBTA, 36.19–48.68 kJ mol-1 for PATA, 36.97-50.82 kJ mol^{-1} MBTA, 38.33-61.66 kJ mol^{-1} for MTMP than that obtained for uninhibited solution (32.82 kJ mol^{-1}).Higher hindrance to corrosion is offered by the presence of additives as indicated by higher value of E_a.

It has already been studied that reduction, very little change or unchanged free energy of activation indicates the happening of chemisorption. Conversely, a comparatively stable value of E_a, i.e. minor change or no change can be associated with mixed mode of adsorption [43]. An advantageous physical or chemical interaction is indicated by upward or downward change of free energy of activation. An inspection of Table 4 confirms that value of E_a regularly increased with increasing

Table 2
Inhibition efficiency comparison of the inhibitors, CBTA, PATA, MBTA and MTMP with some other earlier studied thiazole derivatives.

Inhibitor	Surface	Aggressive media	Inhibitor's concentration (mg L^{-1})	Efficiency			Reference
				E_{WL}%	E_{EIS}%	E_{PDP}%	
CBTA	Mild Steel	1 M HCl	6	82.4	84.4	87.6	–
PATA	–	–	–	90.4	90.2	88.6	–
MBTA	–	–	–	92.8	91.3	90.0	–
MTMP	–	–	–	96.7	93.9	91.8	–
BTMO	Zn	0.1 M HCl	247.2	92.0	86.0	88.0	1
BTCQ	–	–	296.8	91.0	82.0	90.0	1
1	Cu	1 M HNO3	250	66.5	–	–	2
2	–	–	–	68.3	–	–	2
3	–	–	–	82.2	–	–	2
TCA	Mild Steel	0.5 M H2SO4	11313	92.3	89.0	82.0	3
MTT	–	–	11515	93.4	92.1	88.3	3
APT	–	–	19026	98.1	96.8	95.2	3
A1	C-Steel	1 M H2SO4	2.94	59.4	–	66.1	4
A2	–	–	2.76	56.5	–	63.0	4
A3	–	–	2.61	50.4	–	60.0	4
A4	–	–	2.98	32.0	–	39.3	4
A5	–	–	3.10	25.5	–	38.6	4

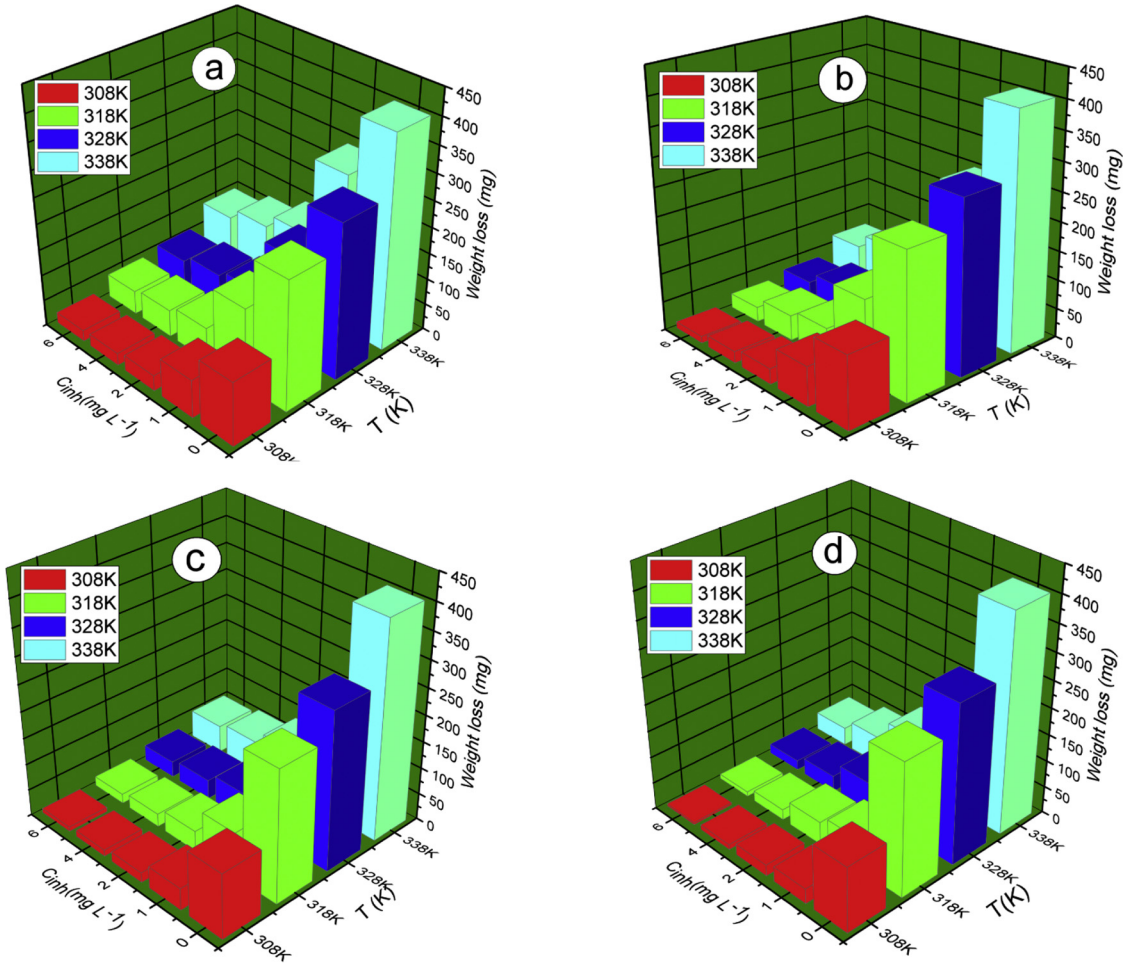

Fig. 3. Weight loss measurement data of (a) MTMP, (b) MBTA, (c) PATA and (d) CBTA at different temperatures.

Table 3
Corrosion parameters obtained from weight loss measurements for mild steel in 1 M HCl with various concentrations of CBTA, PATA, MBTA, and MTMP.

Name of Inhibitor	Concentration of Inhibitor (mg L^{-1})	Mean Weight Loss (mg)	Standard deviation (σ)	E_{WL}%
–	–	122.00	0.39	–
CBTA	1	72.95	0.19	40.2
	2	30.13	0.18	75.3
	4	23.67	0.26	80.6
	6	21.47	0.21	82.4
PATA	1	66.73	0.20	45.3
	2	26.60	0.16	78.2
	4	20.00	0.19	83.6
	6	11.71	0.21	90.4
MBTA	1	41.36	0.09	66.1
	2	18.78	0.16	84.6
	4	12.07	0.11	90.1
	6	08.78	0.14	92.8
MTMP	1	28.30	0.24	76.8
	2	20.98	0.19	82.8
	4	9.64	0.08	92.1
	6	4.02	0.12	96.7

amount of CBTA, PATA, MBTA, and MTMP. A shifting of equilibrium towards desorption of inhibitors at higher temperature is indicated by the rise in E_a.

Riggs and Hurd's [44] mechanism can successfully explained the obtained experimental results. According to this mechanism

$$k_1(1-\theta) + k_2\theta = -\frac{d[Fe]}{dt} \quad (17)$$

Where, θ represents portion of MS surface occupied by additive while k_1 and k_2 represent rate constant of non-inhibited reaction and completely occupied surface area.

In general, adsorption of additive molecule on the metal surface can be written as:

$$M + Add \leftrightarrow M(Add)_{ads} + M^{n+} + ne^{-} + Add \quad (18)$$

Where, M represents metal surface, Add, the additive molecule and $M(Add)_{ads}$, the reaction intermediates (inhibitor adsorbed on the surface).

Initially, when $M(Add)_{ads}$ is not sufficient to cover the metal surface effectively due to low concentration of inhibitor, the rate of metal dissolution is high due to unoccupied active sites of the substrate surface and thereby aggressive ions/molecules are freely adsorbed to cause corrosion. With progressively increasing concentration of inhibitor, formation of compact film takes place due to adsorption of additive molecule and thereby the rate of corrosion started to decrease.

Initially, when rate of adsorption is quite low ($k_2 << 1$), the term $k_2\theta$ might be negligible. On the other hand when inhibitor covered the surface effectively, i.e. θ is quite large (> 0.9), the term $k_1(1-\theta)$ may be insignificant. Thus, at high degree of surface coverage

$$-\frac{d[Fe]}{dt} = k_2\theta \quad (19)$$

Thus, the value of $E_a(-\Delta E_2/RT + \ln\lambda = \ln k_2)$ will be different with respect to that of uninhibited reaction. Thus, the value of E_a may

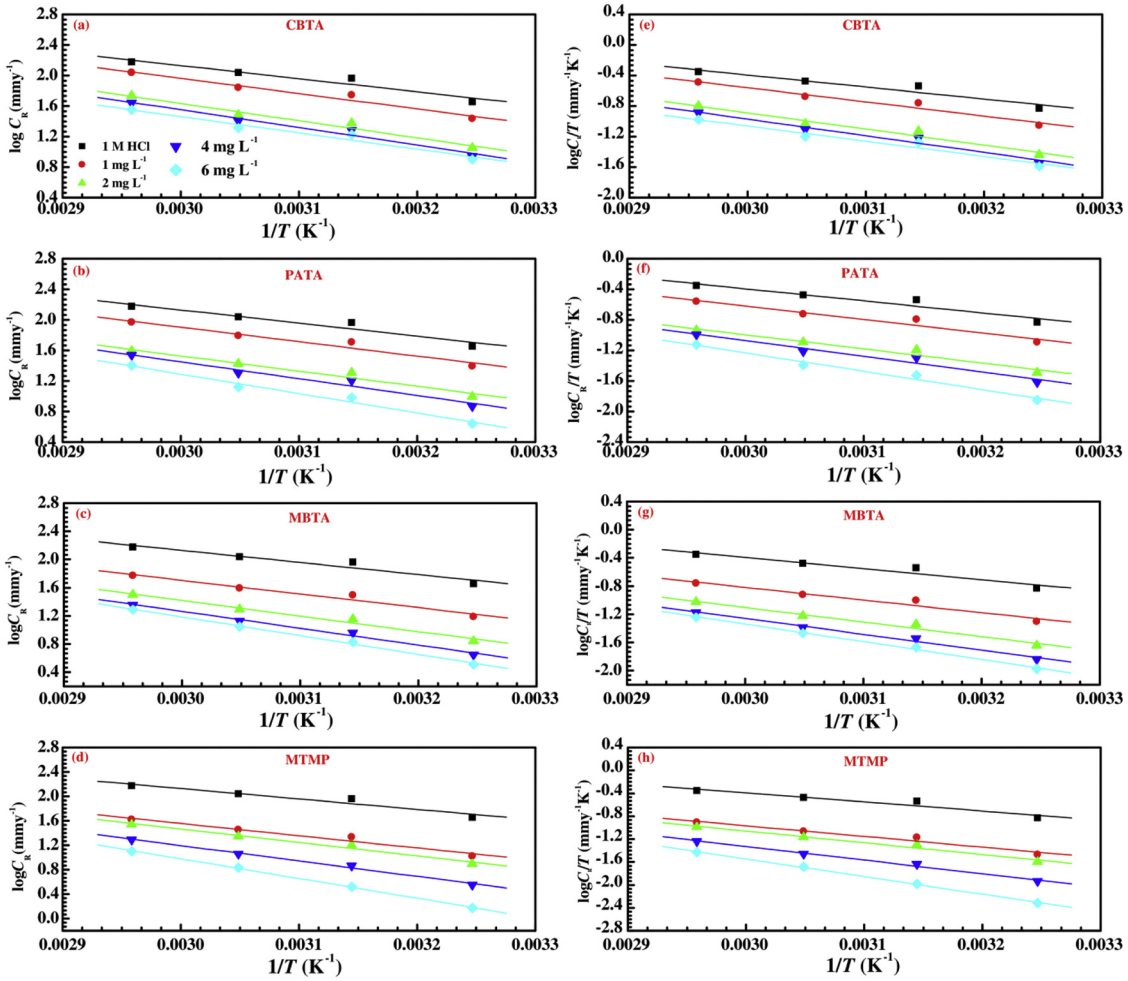

Fig. 4. Arrhenius plots of log C_R vs. $1/T$ and log C_R/T vs. $1/T$ for different inhibitors.

change in both way (when additives covered the surface quite effectively) with respect to non-inhibited reaction.

The variation of E_a (listed in Table 4) with amount of additives confirms dominance of activation parameters in controlling the corrosion.

The graph obtained by plotting log C_R/T vs. $1/T$ provided the values of ΔH^*, and ΔS^* which are listed Table 4. Presence of additives results in to an increase of ΔH^* which suggests that rise in temperature favors the formation of activated complex. Similar trend was noticed with respect to entropy of activation also which indicates increased randomness ongoing from reactant to activated complex. The entropy increment is attributed to increased randomness of solvent molecules [45,46].

Table 4
Activation parameters in presence of different concentrations of inhibitors.

Name of inhibitor	Concentration of inhibitor (mg L^{-1})	E_a (kJ mol^{-1})	λ (mg cm^{-2})	ΔH^* (kJ mol^{-1})	$-\Delta S^*$ (J K^{-1} mol^{-1})
–	–	32.82	1.87×10^7	30.14	114.70
CBTA	1	38.28	9.13×10^7	35.60	101.53
	2	43.00	2.34×10^8	40.31	93.70
	4	44.30	3.10×10^8	41.62	91.35
	6	45.74	3.99×10^8	43.06	90.75
PATA	1	36.19	3.74×10^7	33.51	109.94
	2	38.11	3.16×10^7	35.43	105.35
	4	42.02	1.07×10^8	39.33	100.15
	6	48.68	8.25×10^8	46.00	83.23
MBTA	1	36.97	3.14×10^7	34.29	110.40
	2	42.16	1.05×10^8	39.47	100.32
	4	45.71	2.66×10^8	43.03	92.61
	6	50.82	1.40×10^9	48.14	78.79
MTMP	1	38.33	3.65×10^7	35.65	109.16
	2	42.90	1.07×10^8	40.22	100.20
	4	48.38	5.98×10^8	45.70	85.89
	6	61.66	4.34×10^{10}	58.98	50.26

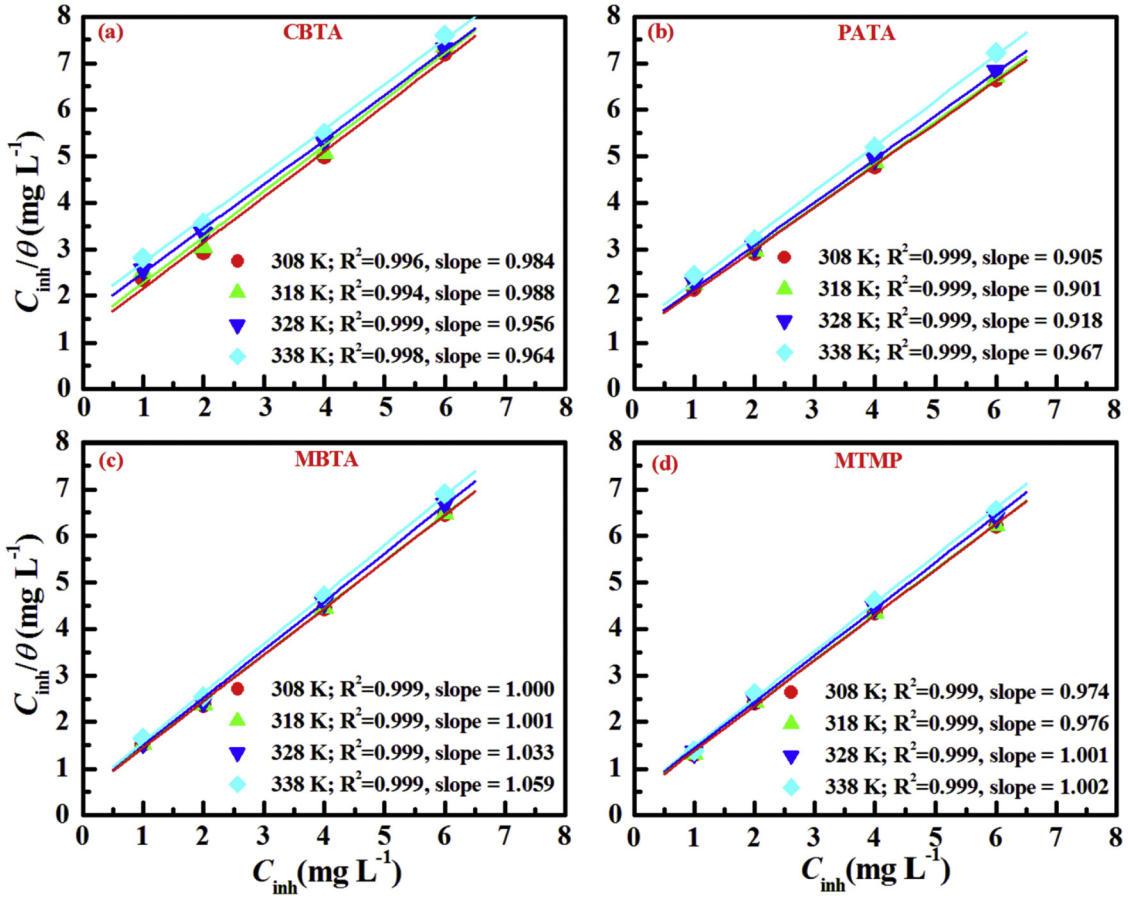

Fig. 5. Langmuir adsorption isotherm for the adsorption of different inhibitors over the surface of mild steel surface.

3.2.4. Surface assimilation behavior of inhibitors

The surface assimilation behavioral study of inhibitors provides mechanistic information about their adsorption [47]. Use of isotherm can provide better understanding about the adsorbing tendency/capacity of an inhibitor's adsorption. Interaction of an additive molecule and MS surface is properly described by applying appropriate isotherm which provides much needed details related to adsorption. Inhibitor molecules adsorbed to the MS (adsorbent) surface through number of interacting forces, viz. intermolecular, electrostatic or through combination of both.

Using data of weight loss experimentations at different temperatures, the surface coverage (θ) for different amounts of additives were calculated. These data were then used to test for fitting of appropriate isotherm. Comparison of linear regression coefficient values obtained for different isotherm suggested that Langmuir isotherm (Fig. 5) can explain the additive's adsorption more appropriately which can be defined by Eq. (20) as [48]:

$$\frac{\theta}{C_{inh}} = \frac{1}{C_{inh}} + K_{ads} \tag{20}$$

Where, C_{inh} symbolizes amount of additive in aggressive solution, θ is part of surface occupied by additive molecule whereas K_{ads} represents distribution of inhibitor between surface and liquid phase (equilibrium constant).

The linearity constant of Langmuir isotherm were found closer to unit value compared to other plausible isotherms, viz. Temkin, Frumkin etc. However, slight deviation in the value of slopes for Langmuir isotherm suggested that it is not perfectly followed in some cases (Fig. 5) which may be resulted because of slight interaction of adsorbed additive molecules which is normally not considered as per original concept of Langmuir's isotherm.

Gibb's free energy for adsorption is related to K_{ads} and water's concentration (C_{H_2O}) in solution as:

$$-2.303RT\log(C_{H_2O}K_{ads}) = \Delta G^0_{ads} \tag{21}$$

Where, all the symbols have their usual meanings.

All the parameters obtained from Eq. (21) are specified as Table 5.The spontaneity of additive's adsorption if confirmed by the negative values of ΔG^0_{ads}.Reasonable higher values of K_{ads} obtained for thiazolyl imines reflects their appreciably good adsorption as K_{ads} is a measure of adsorption strength.

Van't Hoff equation and Gibb's Helmholtz equation can be applied for adsorption process to get adsorption parameters as [49]:

$$\ln K_{ads} = \frac{1}{55.5} + \frac{-\Delta H^0_{ads}}{RT} + \frac{\Delta S^0_{ads}}{R} \tag{22}$$

$$\Delta G^0_{ads} = \Delta H^0_{ads} - T\Delta S^0_{ads} \tag{23}$$

Heat and entropy of adsorption can be found from the graph obtained by plotting $\ln K_{ads}$ vs.$1/T$ or ΔG^0_{ads} vs. T. The value of slope and intercept of both graphs (Fig. 6a-b) provides us the value of heat and entropy of adsorption which is detailed as Table 5. A high degree of consistency is revealed in the results obtained from both graphs.

The value of ΔH^0_{ads} are negative for all the studied inhibitor and hence reflected the exothermic nature of adsorption. The value of ΔH^0_{ads} differentiates interactive forces which resulted in to adsorption of additive molecule. The lower value of ΔH^0_{ads} (< 40 kJ mol^{-1}) is a sign of interaction of inhibitors with MS surface through physical forces while a higher value of ΔH^0_{ads} (> 100 kJ mol^{-1}) signifies chemical nature of interaction [50]. A physical nature of interaction is inferred based on the value of ΔH^0_{ads} found for this study report.

The adsorption in general is preceded with lowering of entropy of

Table 5
Thermodynamic adsorption parameters for the adsorption of different inhibitors over the surface of mild steel.

Name of inhibitor	Concentration of inhibitor (mg L^{-1})	K_{ads} ($10^5 \times M^{-1}$)	$-\Delta H_{ads}$ (kJ mol^{-1})	ΔS_{ads} (J K^{-1} mol^{-1})	$-\Delta G^0_{ads}$ (kJ mol^{-1})	R_L
CBTA	1	–	–	–	–	0.598
	2	–	–	–	–	0.247
	4	–	–	–	–	0.194
	6	1.73	14.15	66.42	41.18	0.176
PATA	1	–	–	–	–	0.588
	2	–	–	–	–	0.247
	4	–	–	–	–	0.188
	6	2.95	24.46	32.58	42.06	0.111
MBTA	1	–	–	–	–	0.343
	2	–	–	–	–	0.156
	4	–	–	–	–	0.100
	6	4.68	27.81	28.93	43.52	0.073
MTMP	1	–	–	–	–	0.223
	2	–	–	–	–	0.144
	4	–	–	–	–	0.075
	6	11.44	28.30	25.01	45.38	0.031

adsorption as adsorption results in to more orderly arrangement of inhibitors. In this study, the value of ΔS^0_{ads} are positive for all the inhibitors. This can be explained by assuming that the adsorption is a substitutional process proceeding as:

$$Add_{(aggressive\ solution)} + xH_2O_{(ads)} \rightleftarrows Add_{(ads)} + xH_2O_{(aggressive\ solution)} \quad (24)$$

In Eq. (24), $Add_{(aggressive\ solution)}$ represents additive molecule in the aggressive solution, $Add_{(ads)}$ that adsorbed on MS surface whereas $H_2O_{(ads)}$ and $H_2O_{(sol)}$ are water molecules in adsorbed condition and in aggressive solution. The factor x represents the degree of substitution of additive molecule, i.e. ability of single additive molecule to substitute x water molecules.

Thus, it can be concluded that the solvent's entropy and additive's entropy both contributes to system's total entropy. Hence rise in system's entropy is simply due to the rise in solvent's entropy [51].

The calculation of an equilibrium parameter (separation factor, R_L) helps us to predict about the nature of adsorption. The relation between adsorption constant (K_{ads}) and equilibrium parameter, R_L, is presented by Eq. (25) as:

$$R_L = \frac{1}{1 + K_{ads} C_{inh}} \quad (25)$$

Where, all the parameters have their usual meanings. The values of calculated R_L listed in Table 5 helps us to predict about the feasibility of adsorption. An irreversible, unfavorable and favorable process is characterized by $R_L = 0$, $R_L > 1$, and $0 < R_L < 1$ respectively [52]. The values of R_L obtained for all the inhibitors confirmed their favorable adsorption on the surface of mild steel. An inclination of adsorption towards chemical nature is specified by decreasing value of R_L with increasing amount of additives.

3.3. Electrochemical investigation

3.3.1. Open circuit potential (OCP)

The thermodynamic tendency of a material to be oxidized electrochemically can be predicted on the basis of their open circuit potential (OCP) [53]. The OCP of mild steel samples immersed in various electrolytic solutions were determined with respect to time for 30 min prior to every electrochemical experiment. The change of OCP measured against concentration of different inhibitors for 30 min time is shown as Fig. 7a–d. The change of OCP did not show any definite pattern and thereby proved the mixed type behavior of the inhibitors.

3.3.2. Potentiostatic electrochemical impedance spectroscopy (PEIS)

Recently, electrochemical impedance spectroscopy (EIS) can be validated as an impressive and accurate method to estimate corrosion rate and thereby study corrosion systems. EIS measures polarization resistance or charge transfer resistance to know the corrosion rate at monitored interface.

The software uses an appropriate equivalent circuit to get best fit for the obtained EIS spectrum. Fitting of appropriate equivalent circuit enables us to get all the EIS parameters.PEIS study of mild steel was carried out in different HCl solutions with varying amount of the different inhibitors, CBTA, PATA, MBTA and MTMP. The results of PEIS

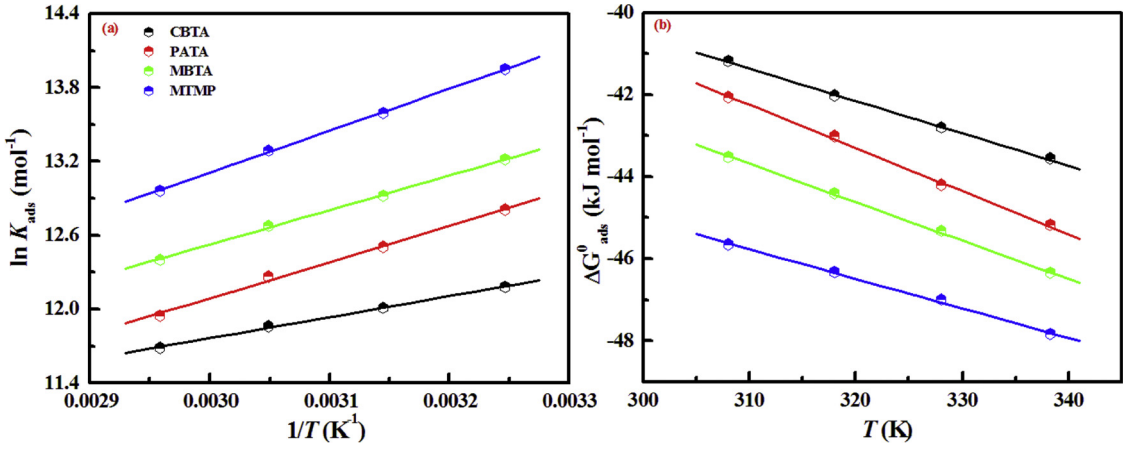

Fig. 6. (a) Plot of ln K_{ads} vs. $1/T$ and (b) $-\Delta G^0_{ads}$ vs. T for different inhibitors.

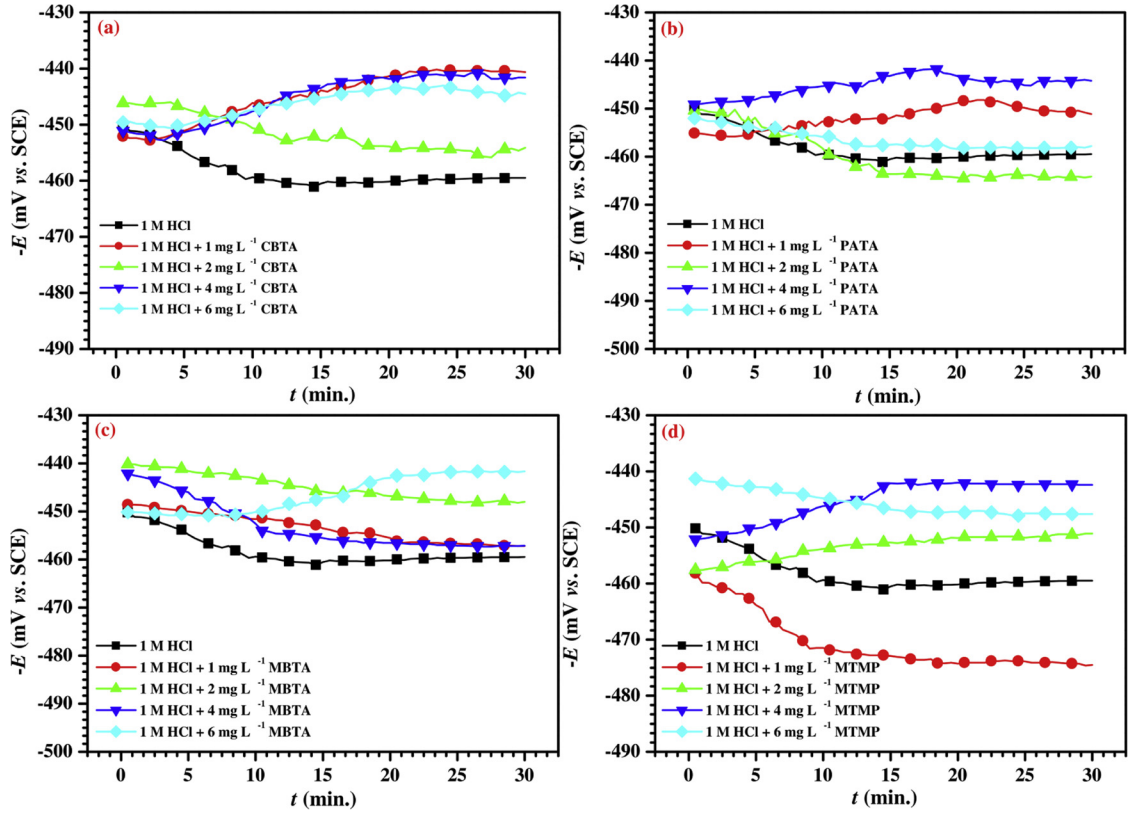

Fig. 7. Variation of open circuit potential against time in the presence of different concentrations of different inhibitors.

are graphically presented as Fig. 8. The Nyquist plots (Fig. 8a-d) revealed that the shape have not affected by the presence of inhibitors while the diameter increased proportionally with inhibitor's concentration. The increase in diameter of the Nyquist plots is explained by the fact that increasing concentration of inhibitors provided improved resistance against corrosion because of the adsorption over the MS surface. The Bode-Phase angle plots are presented as Fig. 8b-l.

The impedance nature of mild steel in bare acid and solution possessing inhibitors, CBTA, PATA, MBTA and MTMP was controlled by combined effect of resistance, capacitance and inductance. However, occurrence of only small portion of Nyquist plot in positive Y-axis emphasized that resistance and capacitance of the system controlled its impedance behavior. This is due to occurrence of electrical double layer or development of oxide film at MS-acid solution interface. The shape of Nyquist plots is depressed semicircles instead of a perfect semi-circle. The depression is associated with roughness as well as inhomogeniety of the surface [54]. The Nyquist plots attained in this study comprises of a capacitive loop at high frequency whereas an inductive loop at lower frequency. These low frequency inductive loops may be assigned to local corrosion (due to adsorption Cl^- ions) at mild steel surface which might be due to the desorption of few inhibitor moieties. However, the increasing size of inductive loop with enhancing the amount of inhibitor is attributed to re-adsorption of charged intermediate species. Thus, desorption-readsorption of inhibitor species on the MS resulted in to large sized inductive loops.

The low value of solution resistance, R_s ($< 1.6\ \Omega\ cm^2$) signifies the stable nature of electrolytic solution while the reducing value of Y_0 with inhibitor's amount indicates that charge accumulation over the mild steel surface is prominently decreased by the increasing amount of inhibitors.

Considering it, Double layer Capacitance (C_{dl}) in the circuit was substituted by constant Phase element (CPE) to obtain more accurate and optimized it. The equivalent electric circuit which consists of solution resistance (R_s), CPE and charge transfer resistance (R_{ct}) linked in series to a parallel sequence of resistance attributed to inductance (R_L) as well as inductance (L) utilized to analyze the impedance information is shown as Fig. 9a and all the impedance results attained by fitting the circuit to the experimental data are given in Table 6. Fig. 9b represents simulated fit data with experimental data obtained for 6 mg L^{-1} MTMP. The Impedance (Z_{CPE}) can be estimated by the following equation:

$$Z_{CPE} = R_s + [1/\{(j\omega)^n Q + 1/(R_{ct} + 1/(1/j\omega L)\}] \quad (26)$$

where, Q represents the magnitude of CPE, j denotes imaginary number ($j^2 = -1$), ω is angular frequency and n denotes phase exponent that represents the extent of irregularity.

Angular frequency (ω) is attained from the Eq. 27 described below at the frequency with the highest imaginary impedance.

$$\omega = (QR_{ct})^{-n} \quad (27)$$

Subsequently, double layer capacitance can be estimated by applying the subsequent relation [55]:

$$C_{dl} = (QR_{ct}^{1-n})^{\frac{1}{n}} \quad (28)$$

Value of n is always between 0 and 1 as it justifies the difference from ideal behavior. As per the Helmholtz model depicted in Eq. 29, double layer capacitance could be linked to the thickness of the electrical double layer which acts as a protective film by following relation:

$$C_{dl} = \frac{\varepsilon\varepsilon_0 A}{d} \quad (29)$$

where, d represents the thickness of the double layer, ε is dielectric constant, ε_0 is vacuum permittivity and A is an area of the electrode.

So, inspection of data revealed that enhancing the amount of the inhibitors brings a gradual reduction in the value of C_{dl} that is because of the depression in local dielectric constant or/and enlargement in thickness of double layer [56]. It results in to enhanced surface coverage by effective adsorption of inhibitor molecules which led to increased inhibition efficiency. The impedance behavior of mild steel is

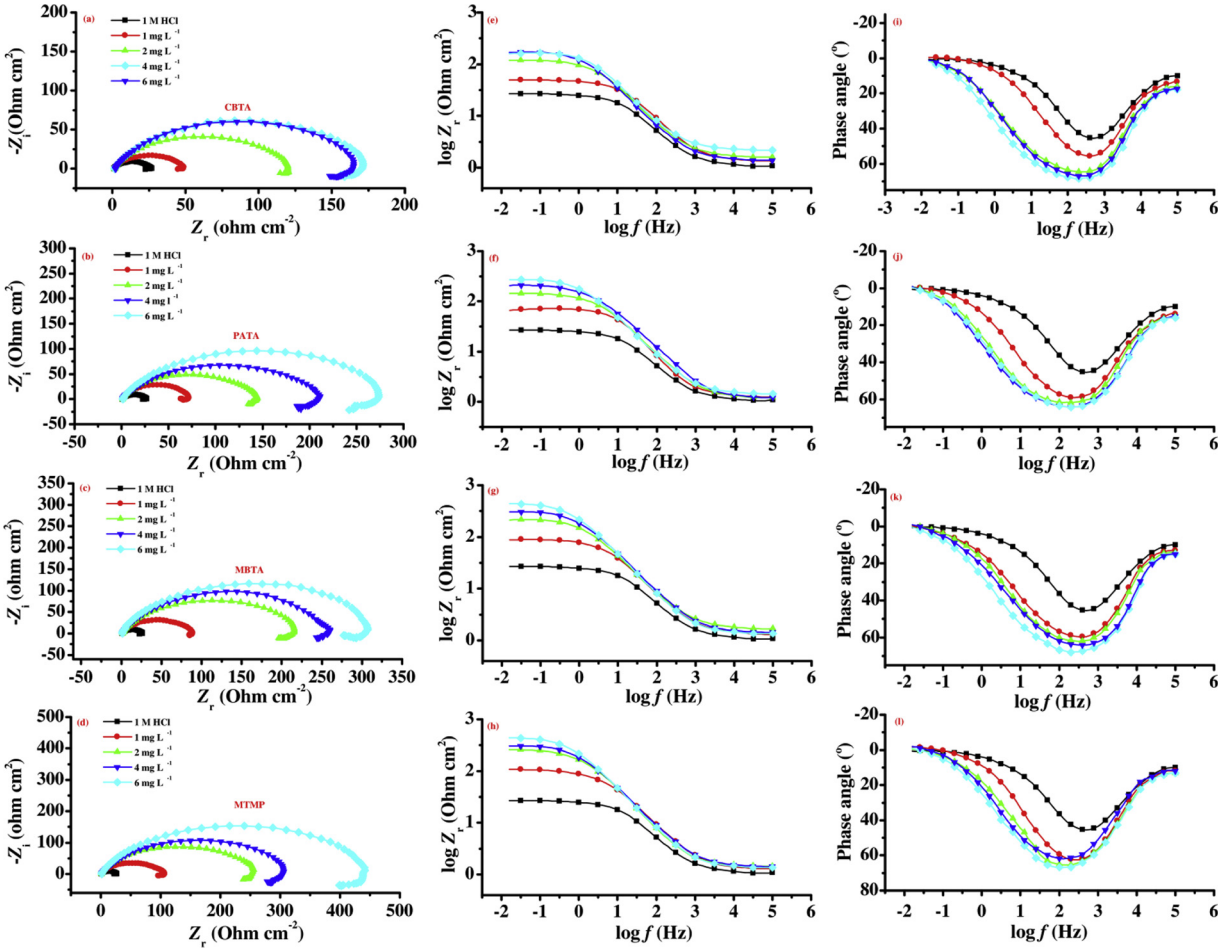

Fig. 8. Nyquist and Bode-Phase angle plots for mild steel in 1 M HCl in presence of different concentrations of different inhibitors.

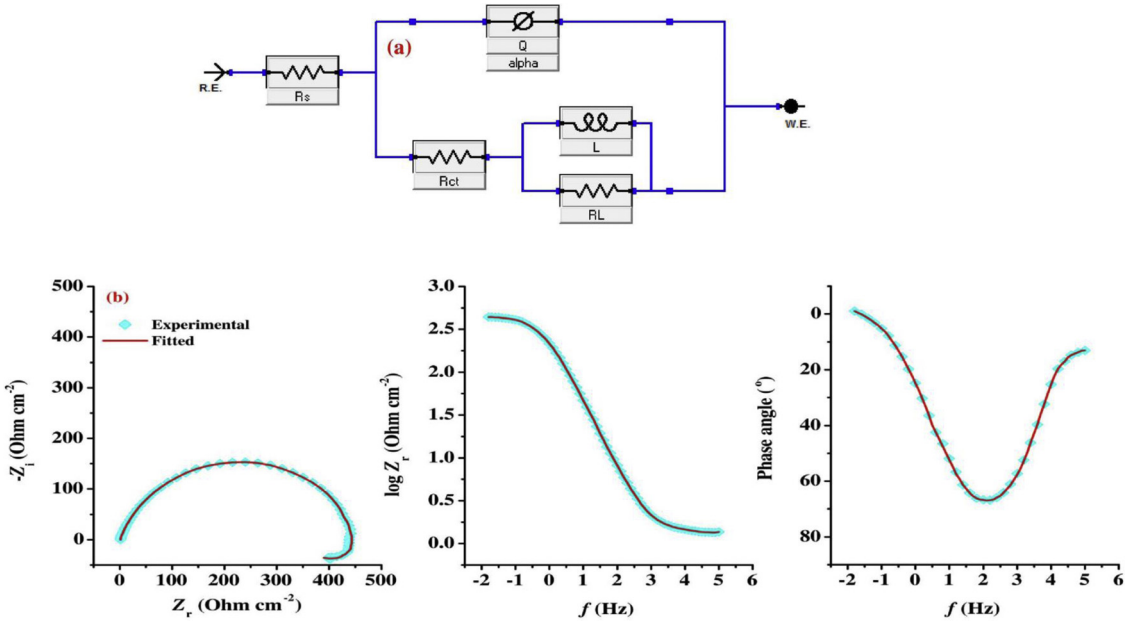

Fig. 9. (a) Equivalent circuit used to fit experimental data (b) fitting of experimental data obtained with 6 mg L^{-1} of MTMP with the equivalent circuits proposed in Fig. 9 (a).

Table 6
EIS parameters of mild steel immersed in 1 M HCl solution with different amount of tested inhibitors.

Name of inhibitor	C_{inh} (mg L^{-1})	R_s (Ωcm^2)	R_{ct} (Ωcm^2)	R_L (Ωcm^2)	n	L (H)	Y_0 ($10^{-6}\Omega^{-1}$ cm^{-2})	C_{dl} (μF cm^{-2})	τ (s)	E_{EIS}%
–	–	0.4	26.8	3.4	0.810	12.9	242.6	74.4	0.0019	–
CBTA	1	1.4	48.6	4.2	0.826	9.9	195.5	73.3	0.0035	44.8
	2	1.6	120.3	5.5	0.838	9.2	151.1	69.6	0.0083	77.7
	4	1.4	165.4	17.6	0.845	8.7	130.3	64.4	0.0106	83.8
	6	1.2	171.6	16.5	0.856	7.8	110.2	56.5	0.0096	84.4
PATA	1	1.3	71.6	8.7	0.826	10.0	182.1	73.0	0.0052	62.5
	2	0.6	144.5	10.8	0.839	8.7	150.3	72.7	0.0105	81.4
	4	1.2	210.2	23.7	0.851	7.9	115.6	60.3	0.0126	87.2
	6	1.4	273.5	32.7	0.860	6.6	95.8	35.5	0.0097	90.2
MBTA	1	1.3	88.7	4.2	0.830	9.8	170.3	72.1	0.0063	69.8
	2	1.6	215.8	21.2	0.840	8.1	130.2	65.9	0.0142	87.6
	4	1.4	260.3	22.0	0.847	7.2	100.9	52.5	0.0136	89.7
	6	1.3	307.2	30.0	0.852	6.5	80.3	42.2	0.0129	91.3
MTMP	1	1.3	106.9	10.0	0.836	8.8	148.3	65.8	0.0070	74.9
	2	1.4	255.8	16.9	0.841	7.7	122.1	63.3	0.0161	89.5
	4	1.3	304.4	28.9	0.845	7.5	100.0	52.7	0.0160	91.2
	6	1.4	441.2	41.8	0.850	6.0	72.2	39.3	0.0173	93.9

largely changed on addition of inhibitor as the diameter of semicircle increased considerably in presence of inhibitor.

The relaxation time i.e. the time in which charge distribution return to equilibrium due to electric chaos or perturbation can be defined as:

$$\tau = C_{dl} R_{ct} \tag{30}$$

where τ signifies relaxation time whereas C_{dl} and R_{ct} denotes double layer capacitance and charge transfer resistance respectively.

The adsorption of inhibitor to reach equilibrium takes some time and since this calculated time (listed in Table 6) is short which resulted in to only time constant.

Fig. 8e-l signifies Bode and phase angle curves in presence of different amount of inhibitors. Both bode and phase angle curves are frequency dependent that provide the information regarding the adsorption of inhibitor which results in to protective film. The increasing maxima of phase angle with increasing inhibitor's concentration assigned to increased capacitive behavior of the system. Also, the shifting of phase angle maxima towards lower frequency in presence of increasing inhibitor concentration assigned to decreased corrosion rate having higher inhibitor's concentration.

3.3.3. Tafel polarization

The potentiodynamic polarization plots of mild steel immersed in different HCl solutions having varying amount of inhibitors, CBTA, PATA, MBTA and MTMP, are presented as Fig. 10a–d. It can be concluded from Fig. 10a-d that the anodic metal dissolution as well as cathodic reaction of hydrogen evolution were suppressed significantly by the presence of inhibitors, CBTA, PATA, MBTA and MTMP. However, suppression of cathodic reaction of hydrogen evolution is more pronounced to that of anodic metal dissolution. All the potentiodynamic polarization parameters attained by extrapolating the polarization plots are shown in Table 7. The larger values of β_c compared to β_a in the studied concentration range of inhibitors as well as their more pronounced change provide the same information that the inhibitors, CBTA, PATA, MBTA and MTMP suppress cathodic reactions in a more effective way than that of anodic metal dissolution reaction. The presence of inhibitors, CBTA, PATA, MBTA and MTMP bring very little change in the value of E_{corr} (< 85 mV) [57] which confirmed the mixed type nature of the inhibitors used in this study.

The corrosion rate could be estimated using corrosion current density as:

$$C_R = 3.27 i_{corr} \left(\frac{\text{Eq.wt.}}{\text{d}}\right) \tag{31}$$

Where, i_{corr} denotes the value of corrosion current density in mA cm^{-2}, Eq. Wt. while d represents the equivalent weight and density of mild steel respectively.

The values of corrosion rate obtained from Eq. 31 are presented in Table 7. The corrosion rate values decreased in the same trend by the presence of inhibitors as from other methods.

3.4. Surface characterization of mild steel

3.4.1. SEM-EDS

The effect of applying inhibitors to the electrolytic solutions can be visualized by scanning the SEM images of mild steel dipped in various electrolytic solutions. The SEM images of mild steel surface before and after immersion in different solutions are depicted in Fig. 11a-f. The morphology of mild steel sample before treating with acid looks smooth (Fig. 11a) which got damaged by maximum extent when it is treated with 1 M HCl solution without any inhibitor (Fig. 11b). The application of inhibitors to the acid solution reduced its aggressiveness significantly as confirmed by the smoother morphology of mild steel obtained after immersing in acid having inhibitors, CBTA, PATA, MBTA and MTMP, separately. The maximum protection was observed when the mild steel sample was treated with MTMP solution (Fig. 11f). The protection of mild steel surface from corrosion is attributed as a result of adsorption of the inhibitor on its surface which could be further affirmed by their EDS spectra presented along with their SEM images. The peaks of N and S are observed in the EDS spectra of mild steel after treating with inhibitors which confirm the adsorption of inhibitors over the metallic surface. The peak of oxygen was observed when the mild steel was treated with bare acid which indicates the formation of oxide. The peaks of O were seen in the presence of all the inhibitors, however, the percentage of O were low with CBTA and PATA. The O peak with CBTA and PATA may be due to atmospheric oxygen to which mild steel got exposed before scanning EDX spectra. The percentage of O increased further in the presence of MBTA and MTMP which is attributed to their oxygen rich structures.

3.4.2. AFM

The atomic force micrographs of mild steel surface taken out of different electrolytic solutions after immersing them for 6 h scanned using atomic force microscope; Model Bruker (Dimension ICON with scan Asyst) and were further analyzed by software Nanoscope analysis 1.8. The AFM images of mild steel samples are demonstrated in Fig. 12a-f. The analysis of atomic force micrographs through Nanoscope analysis 1.8 revealed the average surface roughness of mild steel sample before exposing to acid as 22.2 nm. The mild steel surface got extremely damaged when treated with bare acid as average surface roughness was

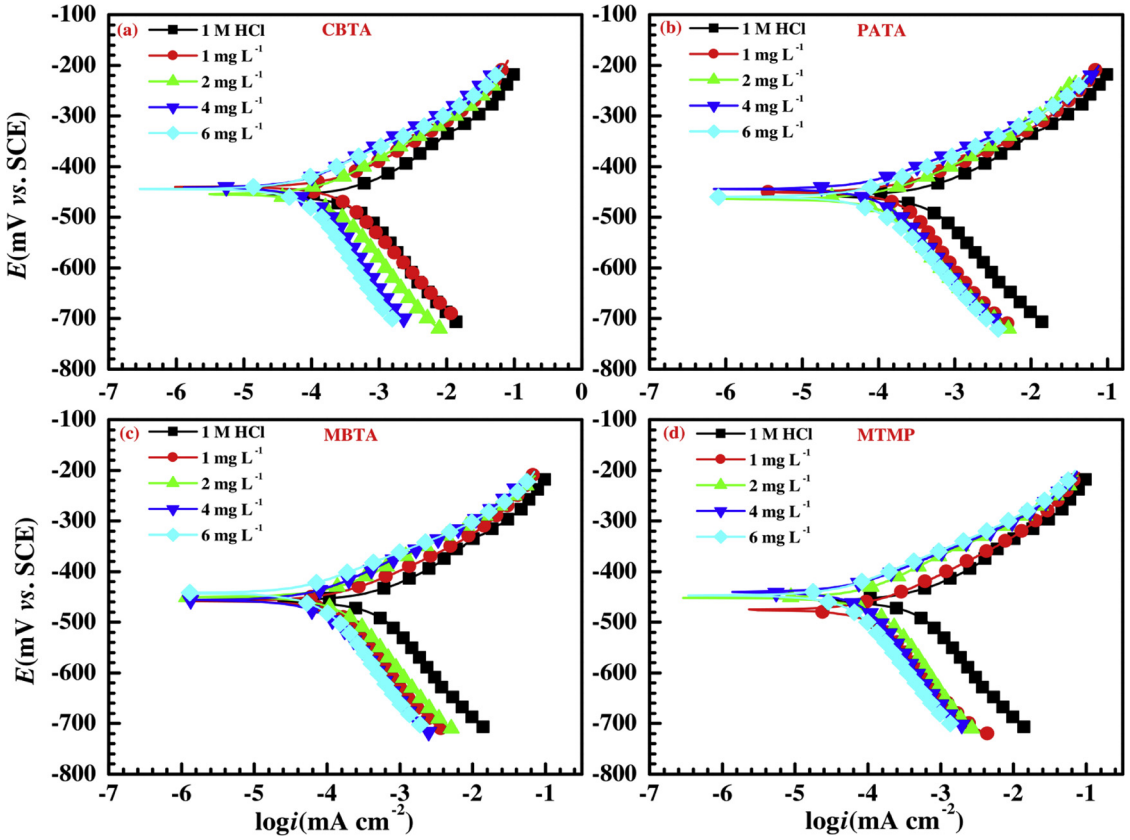

Fig. 10. Tafel polarization curves in absence and presence of different concentration of different inhibitors.

found to increase from 22.2 to 1335 nm. However, the presence of inhibitors brought reduction in average surface roughness of mild steel up to 133, 82.6, 78.0 and 61.5 nm for CBTA, PATA, MBTA and MTMP respectively. The order of average surface roughness was found exactly the same to that of their order of corrosion impeding efficiency, i.e. CBTA < PATA < MBTA < MTMP. This reduction in average surface roughness is resulted because of the effective adsorption of inhibitor over metallic surface that provided barrier for corrosion phenomenon to advance further.

3.4.3. XPS

XPS analysis has been found as a very useful technique to predict about the composition of inhibitor's film formed over the electrode surface because of adsorption. The XPS spectra of the MS surface taken out from the inhibitor (CBTA) solution (immersed for 6 h) are presented as Fig. 13. These spectra are designated to the corresponding species via deconvolution employing XPS peak-Fit 4.1 software.

The C 1s spectrum deconvoluted in to three peaks at 284.77, 286.44 and 288.46 respectively. The peak at 284.77 is assigned to C—C or C–H aromatic bonds and the peaks at 286.44 and 288.46 are assigned for C–N and C–O, C–S respectively.

The Fe 2p shows three peaks; the first one at 710.9 assigned to Fe_2O_3 and Iron oxyhydroxide, i.e. FeOOH. The peak at 714.2 shows the presence of $FeCl_3$ which might be due to corrosive medium while the

Table 7
Potentiodynamic polarization parameters for mild steel in 1 M HCl in absence and presence of different concentrations of inhibitors.

Electrolyte solution	Inhibitor	Concentration (mg L^{-1})	$-E_{corr}$ (mV vs. SCE)	i_{corr} (μA cm^{-2})	β_a (mV dec^{-1})	β_c (mV dec^{-1})	C_R (mmy^{-1})	E_{PDP}%
1 M HCl	–	–	458	563	77	195	6.63	–
	CBTA	1	440	263	80	113	3.09	53.3
		2	454	150	72	160	1.76	73.3
		4	441	90	70	199	1.06	84.0
		6	444	70	68	215	0.82	87.6
	PATA	1	450	226	75	212	2.66	59.8
		2	464	138	77	180	1.62	75.5
		4	444	87	62	172	1.02	84.5
		6	460	64	65	153	0.75	88.6
	MBTA	1	458	158	71	199	1.86	71.9
		2	450	134	73	168	1.57	76.2
		4	456	82	69	173	0.96	85.4
		6	442	56	70	178	0.65	90.0
	MTMP	1	475	123	72	180	1.44	78.1
		2	452	95	71	170	1.11	83.1
		4	440	70	69	188	0.82	87.6
		6	447	46	69	164	0.54	91.8

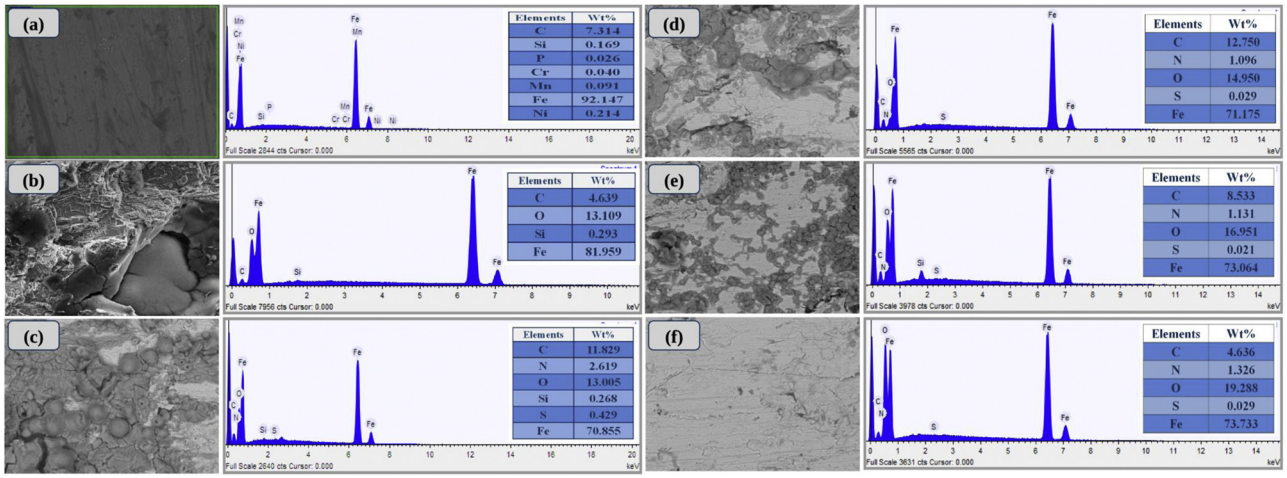

Fig. 11. SEM images and EDX spectra of mild steel surface after immersion in acid solution with different inhibitors.

peak at 727.1 attributed to the formation of α-Fe_2O_3, Fe_3O_4 and FeOOH [58].

The deconvolution of N 1s resulted in to two peaks; first at 399.6 and second at 403.2. The first peak at 399.6 is assigned to C–N bond and aromatic nitrogen present in thiazole ring while other peak at 403.2 is attributed to oxidized form of nitrogen which resulted due to its protonation. This is an indication of positive polarization of nitrogen.

The XPS spectra of O 1s is deconvoluted in to two peaks; one at 529.9 and another at 531.5. The first peak located at 529.9 assigned to O^{2-} associated with Fe^{3+}, i.e. present as Fe_2O_3 while the second one located at 531.5 explained the presence of OH- in FeOOH [53]. Thus, presence of insoluble layer of $Fe_2O_3$and FeOOH prevents ionic diffusion which resulted in to improved corrosion resistance. The S 2p XPS spectra displayed two peaks at 163.8 and 168.4 which represent S—C and S-Fe bond respectively [59]. Thus, existences of these peaks in the XPS spectra of mild steel satisfactorily explain the adsorption of inhibitor, MTMP.

3.5. Theoretical analysis

3.5.1. DFT calculations

Quantum chemical calculations (QCC) and Fukui functions were carried out to establish factors governing inhibitors performance. Frontier molecular orbitals of inhibitor molecules can provide useful data for predicting their interaction with metal surface [60]. Frontier orbital such as HOMO orbitals and LUMO orbitals provides us with a simple method to predict directly the tendency of species to donate or accept electrons. The energy of the HOMO of a molecule is directly linked to the ionization potential and indicates its susceptibility to provide electrons to an assigned acceptor with an empty electron orbital [61]. Likewise, the energy of the HOMO correlates to the ability of a molecule for electron acceptance and it is linked to the electron affinity [62]. On the other hand, the energy gap (ΔE_{gap}) is well known to be associated with the stability and therefore the reactivity of a molecule [63]. A small energy gap value indicates a high reactivity of a molecule and therefore it is expected to be a highly effective corrosion inhibitor. Detailed information's regarding the local reactivity of an inhibitor moiety can be obtained by using Fukui functions as well as dual descriptors [60]. The optimized geometry and the delocalization of the LUMO and HOMO orbitals of all the corrosion inhibitors are

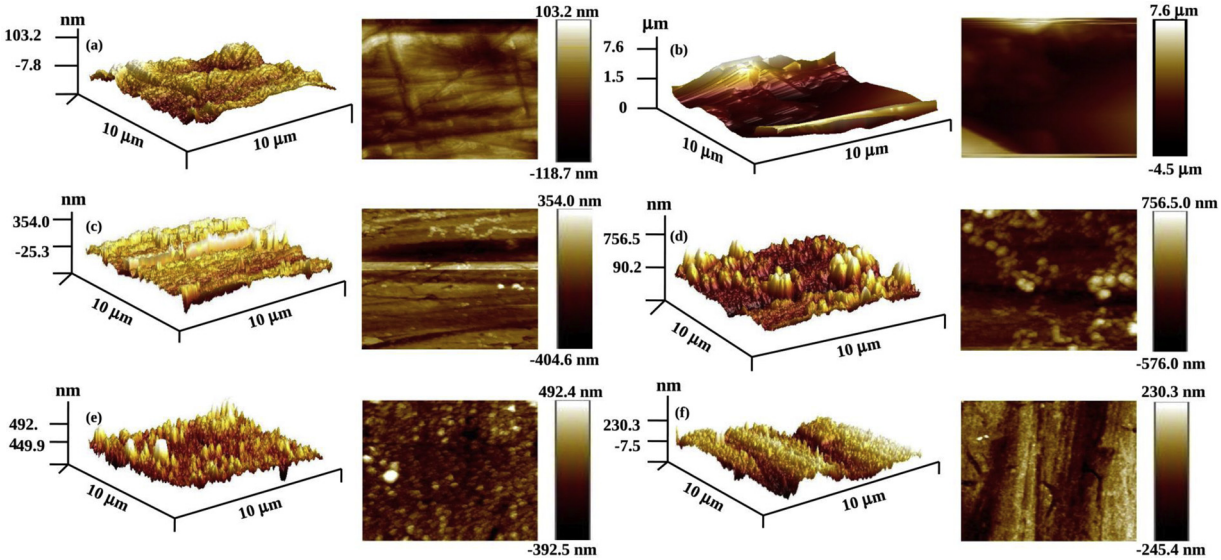

Fig. 12. 2D and 3D atomic force micrographs of mild steel surface (a) before immersion in acid solution, (b) after immersion in 1 M HCl, (c) after immersion in acid solution with MBTA, (d) with CBTA, (e) PATA and (f) with MTMP.

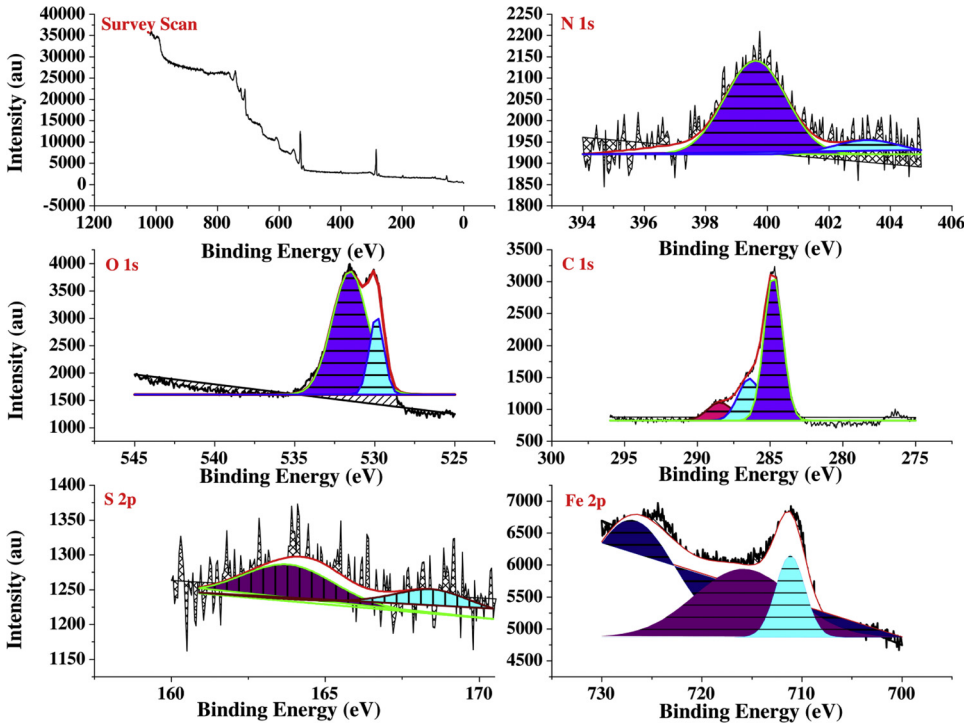

Fig. 13. XPS spectra of mild steel after immersion in acid solution with MTMP.

presented in Fig. 14. Table 8 lists some of quantum chemical parameters. The functional groups have remarkable effects on the inhibition performance of corrosion inhibitors [62]. Such effects can be first assessed by HOMO and LUMO orbitals distribution, which is the graphical representation of frontier orbital energies. While all Schiff basses have a common structure, they differ from each other by the presence or absence of chloride, methoxy, and hydroxyl groups. Fig. 14 shows that the isodensity in HOMO and LUMO orbitals of all molecules is distributed on the whole molecular moiety. It is well observed that thiazole and Schiff base moieties conserve their high-dispersed HOMO and LUMO densities in all compounds. This makes us assume that all compounds should have strong electron accepting and electron

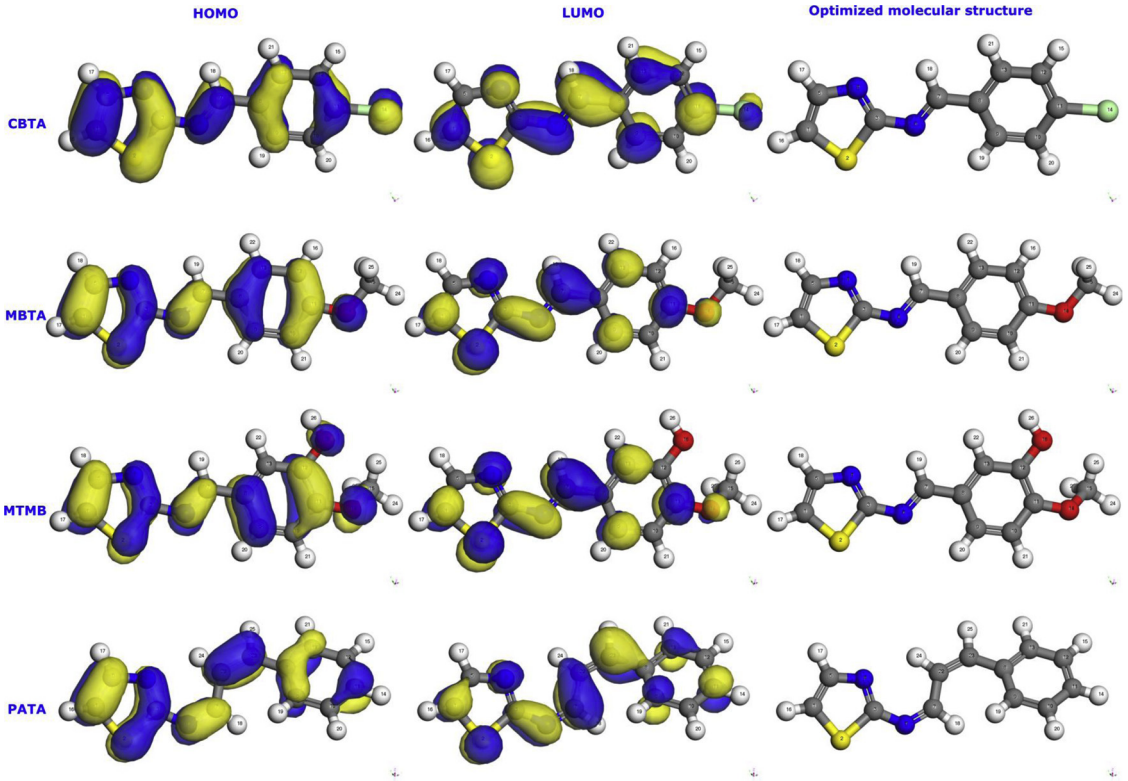

Fig. 14. Optimized molecular structure and frontier molecule orbital density distributions for investigated compounds obtained from DFT calculations.

Table 8
Computed quantum chemical parameters for four inhibitor molecules using DFT method.

Inhibitors	E_{HOMO} (eV)	E_{LUMO} (eV)	ΔE (eV)	ΔN_{110}
CBTA	−5.382	−2.956	2.426	0.268
PATA	−5.248	−3.075	2.173	0.303
MBTA	−5.091	−2.711	2.380	0.386
MTMP	−5.076	−2.778	2.298	0.388

donating abilities since these moieties are well known by their high inhibitive effect. By looking at the effect of functional groups on HOMO-LUMO orbitals distribution, only small changes can be observed. Functional groups like methoxy and hydroxyl, usually, possess strong outcome on the inhibitor reactivity. However, such effect is not well expressed by frontier orbitals distribution.

Quantum chemical parameters can give us a more accurate prediction on both the reactivity of each compound and the effect of its functional groups. It has been reported that high HOMO energy value results in stronger electron-donating tendency, whereas lesser LUMO energy depicts higher electron-accepting ability [64]. By visualizing the data in Table 8, it could be observed that the electron-donating tendency follows the order of MTMP > MBTA > PATA > CBTA. We believe that in these compounds the functional groups can greatly affect their electron-donating ability, thus their inhibitive performance. Compounds associated with –Cl has less donating effect compared to $-OCH_3$ or $-OH$ resulting in lower inhibition efficiency. The dependence of the electron-donating ability on the functional groups can be also expressed by ΔN values. Results in Table 8 describes that, as the electron donating tendency of compounds enhanced, the ΔN values increments as well. All results match well the corresponding experimental results. However, when we look at the LUMO energy values, a different picture emerges. The electron-accepting tendency follows the order of PATA > CBTA > MTMP > MBTA. It seems that compounds with methoxy and/or hydroxyl groups have a less electron accepting power compared to other compounds. The energy difference between E_{HOMO} and E_{LUMO} known as energy gap is an important quantum chemical parameter. Its smaller value results more impulsive shape and heavier tail. The smaller value depicts that the molecule has greater reactivity, thus higher adsorption ability. Like LUMO energy values, the energy gap results are not consistent with experimental observations. Hence, there is greater evidence for a closer relationship between the electron-donating power and inhibitor performance. For further investigation of the inhibitors' reactivity, local reactivity descriptors like Fukui functions and the dual descriptor has been determined.

The electrophilic and nucleophilic condensed Fukui functions have been used to find the reactivity of every atom in the molecule [65]. The atomic sites that have highest values are prone for nucleophilic and electrophilic attack; respectively [60].The dual descriptor is a vital method for illustrating the nucleophilic and electrophilic attack in a precise way. An atomic site having a positive dual descriptor indicates more susceptibility for nucleophilic attack whereas negative dual descriptor illustrates the proclivity for electrophilic attack. Results are listed in Table 9. Fukui functions distribution can provide key insights into the inhibitors' reactivity, which, on one hand, allows efficient prediction of the inhibition performance and which, on the other hand, allows one to obtain more accurate data on contribution of each reactive site in term of its donation or acceptation power. The data in Table 9 demonstrates that the number of susceptible sites for electrophilic attack follows the order of MTMP > MBTA > PATA > CBTA whereas the susceptible sites for nucleophilic attack follow the order of PATA = CBTA > MBTA > MTMP. These results confirm once again our hypothesis that electron-donating power greatly contribute to the increase in inhibitor performance. Fukui function outcomes also demonstrates that the substituted phenyl in MTMP and MBTA compounds has widespread electrophilic sites compared to other compounds. Furthermore, the thiazole moiety in PATA and CBTA has an electrophilic character, but when we add methoxy and/or hydroxy groups to inhibitors, this property nearly disappear and tend to have nucleophilic character. In case of adsorption centers, for instance, Table 9 reveals that the atomic sites C(12), O(14) and O(16) of MTMP would be the most prone to be attacked by an electrophile site, while in the case of MPTA, C(1), C(5) and O(14) are the atomic sites which are likely to be subject to potential electrophile attack. Considering the electrophilic sites, the S(2), N(6) and C(7) in both MTMP and MPTA are the atomic sites that likely to be attacked by a nucleophilic site. It is clear that the thiazole moiety is the main responsible on inhibition efficiency of PATA and CBTA whereas the addition of strong electron donating functional groups to MTMP and MBTA increases the reactivity of the whole molecule, thus better inhibition efficiency.

3.5.2. Molecular motion simulations (MMS)

Although many DFT calculations have been reported, however a fully understanding of the interactions between inhibitors and a metal surface could not be achieved by these calculations. In this situation then simulation methods, especially using molecular dynamics have become a promising technique for studying corrosion inhibition. A very good assessment of inhibitors' adsorption over the steel substrate can be obtained by simulating the interaction of these compounds with metal surface in presence of corrosive particles like water molecules, hydronium, and chlorine ions [66]. These insights can aid in better

Table 9
Output obtained from MD simulation for adsorption of inhibitors on Fe (1 1 0) surface.

Inhibitor MTMP	f_k^+	f_k^-	$\Delta f(k)$	Inhibitor MBTA	f_k^+	f_k^-	$\Delta f(k)$	Inhibitor CBTA	f_k^+	f_k^-	$\Delta f(k)$	Inhibitor PATA	f_k^+	f_k^-	$\Delta f(k)$
C(1)	5.7	6.7	−1	C(1)	5.7	8.2	−2.5	C(1)	5.7	10.1	−4.4	C(1)	5.2	8.3	−3.1
S(2)	11.8	9.3	2.5	S(2)	12.3	10.9	1.4	S(2)	11.8	13.2	−1.4	S(2)	10.5	12.0	−1.5
C(3)	4.2	3.4	0.8	C(3)	4.3	4.3	0.0	C(3)	3.7	6.2	−2.5	C(3)	3.2	4.6	−1.4
N(4)	6.4	4.3	2.1	N(4)	6.4	5.1	1.3	N(4)	6.1	5.8	0.3	N(4)	5.3	4.6	0.7
C(5)	3.6	5.4	−1.8	C(5)	3.6	6.7	−3.1	C(5)	3.7	8.8	−5.1	C(5)	3.4	7.4	−4.0
N(6)	8.3	5.6	2.7	N(6)	8.0	6.4	1.6	N(6)	8.4	5.9	2.5	N(6)	8.2	6.6	1.6
C(7)	12.1	3.8	8.3	C(7)	12.1	4.5	7.6	C(7)	11.6	6.0	5.6	C(7)	9.3	5.0	4.3
C(8)	3.2	5.0	−1.8	C(8)	3.0	5.3	−2.3	C(8)	3.5	3.5	0.0	C(8)	2.0	2.7	−0.7
C(9)	4.9	5.6	−0.7	C(9)	4.8	3.5	1.3	C(9)	5.1	3.5	1.6	C(9)	3.4	2.9	0.5
C(10)	3.1	3.7	−0.6	C(10)	3.1	4.0	−0.9	C(10)	3.1	2.7	0.4	C(10)	2.4	2.4	0.0
C(11)	5.0	6.0	−1	C(11)	5.0	4.9	0.1	C(11)	5.2	4.2	1.0	C(11)	4.5	4.5	0.0
C(12)	2.5	4.8	−2.3	C(12)	3.0	4.3	−1.3	C(12)	3.3	2.9	0.4	C(12)	2.4	2.3	0.1
C(13)	4.8	3.2	1.6	C(13)	5.0	4.2	0.8	C(13)	4.7	3.6	1.1	C(13)	3.4	3.3	0.1
O(14)	2.9	6.3	−3.4	O(14)	3.2	6.1	−2.9	O(14)	6.9	7.2	−0.3	C(22)	5.5	6.0	−0.5
C(15)	1.0	1.8	−0.8	C(15)	0.9	1.5	−0.6					C(23)	9.8	6.7	3.1
O(16)	1.8	5.1	−3.3												

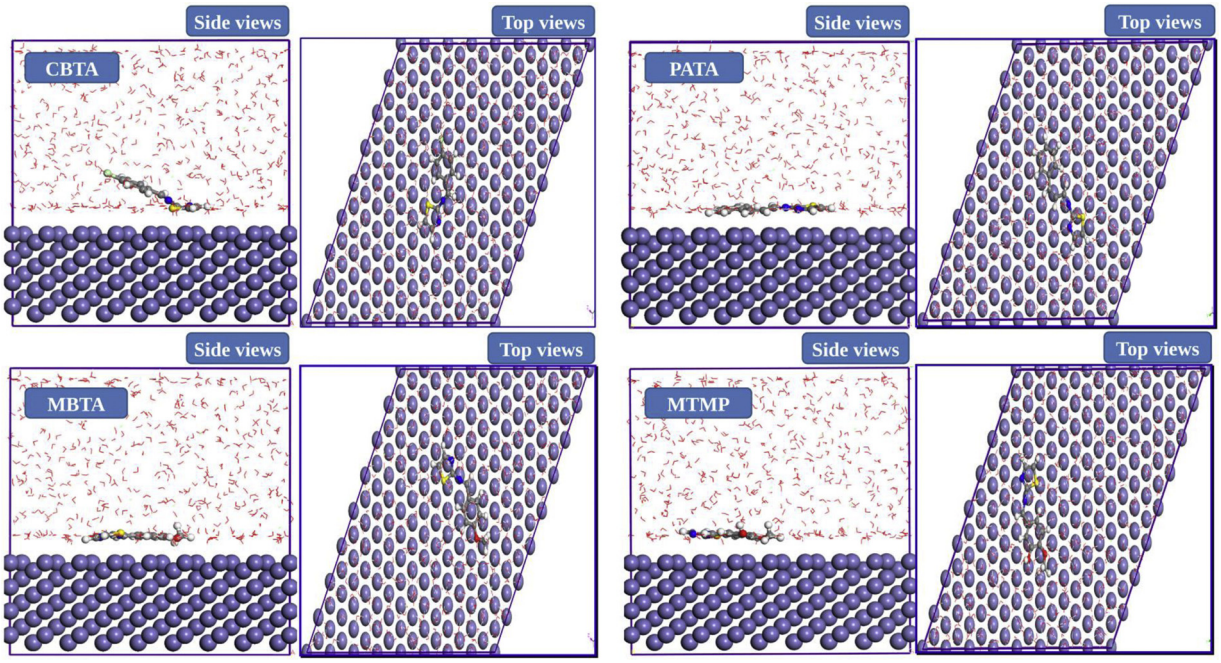

Fig. 15. Side views and top views of the final adsorption of inhibitor molecules on the Fe (110) surface in presence of solvent species.

Table 10
MD parameters for four compounds adsorbed on the Fe (110) surface in presence of solvent species.

Simulation Models	Interaction Energy (kJ mol^{-1})
MTMP	−613.87
MBTA	−598.22
CBTA	−254.08
PATA	−493.69

understanding and prediction of inhibitor-metal interactions, and knowing which factors to consider when designing synthetic corrosion inhibitors. These insights could be attained from MDS that appeared as an effective modeling strategy to understand the mechanism of corrosion inhibition [67,68]. The primary motive of addition of the corrosive molecules is to mimic the actual corrosion phenomenon as precisely as feasible. Fig. 15 represents respectively side and top descriptions of optimized adsorption configurations of four inhibitor species on Fe (110) surface. Within the time period of 2000 ps, simulations were run until an equilibrium condition is reached, then, interaction energies were determined by estimating the single point energies of all system constituents [69]. The interaction energy of all compounds is listed in Table 10.

From the results in Fig.15, it is clearly observed that inhibitor molecules of all compounds, except CBTA, adhered to Fe (110) plane with flat orientation relative to surface. Indeed, parallel disposition can facilitate interactions with the metal surface and, more importantly, the surface coverage rate will be high. In this situation, the possibility for donor-acceptor interactions of the lone pair-electron/π-electrons of reactive positions in inhibitors with the vacant d-orbitals electrons of iron atoms will be increased, thus resulting into the development of a compact adsorption layer. For CBTA, the thiazole has closer contact with Fe (110) plane while the chloro-phenyl is directed toward the solvent layer, and hence the inhibition performance of CBTA is mainly due to its thiazole moiety. This is in agreement with the theoretical outcomes, which illustrates that the thiazole moiety is the most reactive part of CBTA and PATA molecules. Visual inspection of MD results is useful in getting general information about the adsorption profile of inhibitors. However, the interactive forces between Fe (110) plane and inhibitor molecules are significant in determining their adsorption strength, thereby allowing accurate assessment of their performance as corrosion inhibitors.

The interactive forces of inhibitors can be estimated by calculating their interaction energy in contact with the metallic surface. Higher interaction energy can reflect a strong adsorption of an inhibitor species with the iron surface [69]. The similar results can be attained using the binding energy ($E_{binding} = -E_{interaction}$) values. Inhibitors possessing larger binding energy demonstrated larger adsorption tendency [66]. Therefore, from the aspect of interactive force, with the increase of binding energy, the inhibition performance will increase and high inhibition efficiency would be expected. Results in Table 10 shows that, in general, all inhibitor molecules have strong interaction energy. The interaction energy value follows the order of MTMP > MBTA > PATA > CBTA, which is in good agreement with experimental outcomes. Correlating these results with the quantum chemical results, one could understand the inhibitor performance as a direct consequence of the electron donating power accompanied by the effect of the conformation of inhibitors on the iron surface. Once again, we could observe that the addition of chlorine resulted in noticeable differences in the inhibitive activity of CBTA while the addition of various functional groups like methoxy and/or hydroxyl significantly improve the corrosion inhibition efficacy. It should be noted that the results attained using MMS were found to be consistent with the experimental data.

3.6. Mechanism of inhibition

Generally, adsorption plays a vital role in corrosion inhibition by use of organic substances as they are easily adsorbed on the surface and prohibits further corrosion. The results discussed so far supported this mechanism for the case of thiazolyl imines also. Usually, inhibitors may interact to the metal surface in numerous following ways in order to get adsorbed on the surface [70,71]:

- Electrostatic interaction between diff ;erently charged species, i.e. inhibitors and metallic surface,
- Non-bonded electrons of inhibitor molecules with vacant metal orbitals,
- Similarly unsaturation of inhibitor may also participate, i.e. π-

electrons with the vacant metal orbitals and

- Back-bonding or retro-donation. Inhibitor molecules and metal surface can show interaction in such way also.

Based on the above facts it may be comprehended that the conclusive factors for adsorption and subsequently anticorrosion tendency are the molecular structure as well as the electronic properties of an inhibitor molecule. Experimental and theoretical estimations provides an overall picture of the corrosion inhibition mechanism and additionally the nature of inhibitors − Fe interactions. Furthermore, in the presence of HCl solution, inhibitor molecules are easily prone to protonation, which is validated by XPS studies. This suggested that the pre-adsorbed Cl^- ions will be attracted to the protonated inhibitor molecules as an initial step in the adsorption phenomenon [72]. Looking deeper, it is clear that chemisorption is the predominant adsorption mechanism, but it cannot be ruled out that weak physisorption can also occur. Chemisorption takes place through the lone pairs of electrons of heteroatoms and conjugated double bonds.

4. Conclusions

The thiazolyl imines were found to show excellent corrosion impeding behavior as compared to already reported thiazole derivatives against corrosion of mild steel in 1 M HCl. The corrosion rate controlled primarily by activation process. The value of dimensionless separation factor (R_L) predicted that the inhibitors are favorably adsorbed on the surface of mild steel. The shifting of phase angle maxima towards lower frequency in presence of increasing inhibitor concentration assigned to decreased corrosion rate having higher inhibitor's concentration. The Tafel polarization concluded mixed type nature of the inhibitors. The surface characterizations, viz. EDX and XPS explained the adsorption of inhibitor perfectly. All the experimental results are well complemented by theoretical study.

Applications of studied inhibitors for the reduction of acidic corrosion in the petroleum and gas industry will be beneficial in terms of enabling safer operations and managing cost savings. The future research in this field might be explored in the direction of the work related to the scale-up experiments for industrial applications so as to commercialize these inhibitors and effectively substitute the conventional inhibitors presently used for controlling corrosion. Additionally, the work on the studies of real industrial effluent or real life situations is restricted.

Declaration of interest statement

We wish to confirm that there are no known conflicts of interest associated with this publication and there has been no financial support for this work that could have influenced its outcome.

CRediT authorship contribution statement

Ashish Kumar Singh: Conceptualization, Writing - original draft, Writing - review & editing, Data curation, Supervision. **Bhawna Chugh:** Methodology, Writing - original draft. **Sanjeeve Thakur:** Formal analysis, Resources, Supervision. **Balaram Pani:** Formal analysis. **Hassane Lgaz:** Methodology, Software, Writing - original draft. **Ill-Min Chung:** Methodology, Software, Writing - original draft. **Shweta Pal:** Data curation, Methodology. **Rajiv Prakash:** Data curation, Methodology, Resources, Validation.

Acknowledgement

All the authors are thankful to their institutions for providing platform to carry out this research work. We are also thankful to our all the colleagues who have been directly or indirectly involved in this project. The authors are immensely grateful to reviewers for their comments that greatly improved the manuscript.

Appendix A. Supplementary data

Supplementary material related to this article can be found, in the online version, at doi:https://doi.org/10.1016/j.colsurfa.2020.124824.

References

[1] International Measures of Prevention, Application and Economics of Corrosion Technologies Study, NACE-International-Report, 2016.
[2] F.E. Wang, Bonding Theory for Metals and Alloys, second ed., (2019), pp. 157–191, https://doi.org/10.1016/B978-0-444-64201-1.00006-3.
[3] M.A. El-Reedy, Offshore Structures: Design, Construction and Maintenance, first ed., Gulf Professional Publishing, 2012.
[4] P. Shaw, I.B. Obot, M. Yadav, Functionalized 2-hydrazinobenzothiazole with carbohydrates as a corrosion inhibitor: electrochemical, XPS, DFT and Monte Carlo simulation studies, Mater. Chem. Front. 3 (2019) 931–940, https://doi.org/10.1039/C9QM00096H.
[5] A.K. Singh, B. Chugh, S.K. Saha, P. Banerjee, E.E. Ebenso, S. Thakur, B. Pani, Evaluation of anti-corrosion performance of an expired semi synthetic antibiotic cefdinir for mild steel in 1 M HCl medium: an experimental and theoretical study, Results Phys. 14 (2019) 102383, , https://doi.org/10.1016/j.rinp.2019.102383.
[6] N. Arshad, A.K. Singh, B. Chugh, M. Akram, F. Perveen, I. Rasheed, F. Altaf, P.A. Channar, A. Saeed, Experimental, theoretical, and surface study for corrosion inhibition of mild steel in 1 M HCl by using synthetic anti-biotic derivatives, Ionics (2019), https://doi.org/10.1007/s11581-019-03028-y.
[7] A.A. Al-Sarawy, A.S. Fouda, W.A.S. El-Dein, Some thiazole derivatives as corrosion inhibitors for carbon steel in acidic medium, Desalination 229 (2008) 279–293, https://doi.org/10.1016/j.desal.2007.09.013.
[8] M. Yadav, D. Sharma, S. Kumar, Thiazole derivatives as efficient corrosion inhibitor for oil-well tubular steel in hydrochloric acid solution, Korean J. Chem. Eng. 32 (2015) 993–1000, https://doi.org/10.1007/s11814-014-0275-0.
[9] T.K. Chaitra, K. N.Mohana, H.C. Tandon, Study of new thiazole based pyridine derivatives as potential corrosion inhibitors for mild steel: theoretical and experimental approach, Int. J. Corros. 2016 (2016) 1–21, https://doi.org/10.1155/2016/9532809.
[10] L.M. Tao, C.H. Li, J. Chen, H. Liu, Cobalt(III)-catalyzed oxidative annulation of Benzaldehydes with internal alkynes via C−H functionalization in poly(ethylene glycol), J. Org. Chem. 84 (2019) 6807–6812, https://doi.org/10.1021/acs.joc.9b00580.
[11] T.X. Liu, F.B. Li, D.B. Zhou, G.W. Wang, Ferric perchlorate promoted reaction of [60]fullerene with N-sulfonyl aldimines: synthesis and functionalization of fulleroxazolidines, J. Org. Chem. 80 (2015) 11986–11992, https://doi.org/10.1021/acs.joc.5b01868.
[12] M. Tursky, L.L.R. Lorentz-Petersen, L.B. Olsen, R. Madsen, Iridium- and ruthenium-catalysed synthesis of 2,3-disubstituted indoles from anilines and vicinal diols, Org. Biomol. Chem. 8 (2010) 5576–5582, https://doi.org/10.1039/C0OB00106F.
[13] A.D. Hoz, A. Díaz-Ortiza, A. Morenoa, Microwaves in organic synthesis. Thermal and non-thermal microwave effects, Chem. Soc. Rev. 34 (2005) 164–178, https://doi.org/10.1039/B411438H.
[14] T.J. Mason, Ultrasound in synthetic organic chemistry, Chem. Soc. Rev. 26 (1997) 443–451, https://doi.org/10.1039/CS9972600443.
[15] A.K. Singh, S. Thakur, B. Pani, G. Singh, Green synthesis and corrosion inhibition study of 2-amino-N′-((thiophen-2-yl) methylene) benzohydrazide, New J. Chem. 42 (2018) 2113–2124, https://doi.org/10.1039/c7nj04162d.
[16] B. Chugh, A.K. Singh, D. Poddar, S. Thakur, B. Pani, P. Jain, Relation of degree of substitution and metal protecting ability of cinnamaldehyde modified chitosan, Carbohydr. Polym. 234 (2020) 115945, , https://doi.org/10.1016/j.carbpol.2020.115945.
[17] ASTM G1, Standard Practice for Preparing, Cleaning, and Evaluating Corrosion Test Specimens, (1999).
[18] A.K. Singh, S. Thakur, B. Pani, E.E. Ebenso, M.A. Quraishi, A.K. Pandey, 2-hydroxy-N′-((Thiophene-2-yl)methylene)benzohydrazide:ultrasound-assisted synthesis and corrosion inhibition study, ACS Omega 3 (2018) 4695–4705, https://doi.org/10.1021/acsomega.8b00003.
[19] V.P. Singh, M. Mishra, K. Tiwari, A.K. Singh, Synthesis, structural and corrosion inhibition studies on Mn(II), Cu(II) andZn(II) complexes with a Schiff base derived from 2-hydroxypropiophenone, Polyhedron 77 (2014) 57–65, https://doi.org/10.1016/j.poly.2014.04.003.
[20] J. Zhang, L. Zhang, G. Tao, A novel and high-efficiency inhibitor of 5-(4-methoxyphenyl)-3h-1,2-dithiole-3-thione for copper corrosion inhibition in sulfuric acid at different temperatures, J. Mol. Liq. 272 (2018) 369–379, https://doi.org/10.1016/j.molliq.2018.09.095.
[21] N. Chafai, S. Chafaa, K. Benbouguerra, A. Hellal, M. Mehri, Synthesis, spectral analysis, anti-corrosive activity and theoretical study of an aromatic hydrazone derivative, J. Mol. Struct. 1181 (2019) 83–92, https://doi.org/10.1016/j.molstruc.2018.12.073.
[22] Materials Studio, Revision 6.0, Accelrys Inc., San Diego, USA, 2013.
[23] B. Delley, From molecules to solids with the DMol3 approach, J. Chem. Phys. 113 (2000) 7756–7764, https://doi.org/10.1063/1.1316015.
[24] J.P. Perdew, K. Burke, M. Ernzerhof, Generalized gradient approximation made simple, Phys. Rev. Lett. 77 (1996) 3865–3868, https://doi.org/10.1103/

PhysRevLett.78.1396.
[25] A. Klamt, G. Schüürmann, COSMO: a new approach to dielectric screening in solvents with explicit expressions for the screening energy and its gradient, J. Chem. Soc. Perkin Trans. 2 (1993) 799–805, https://doi.org/10.1039/P29930000799.
[26] M.J. Dewar, W. Thiel, Ground states of molecules. 38. The MNDO method. Approximations and parameters, J. Am. Chem. Soc. 99 (1977) 4899–4907.
[27] S. Martinez, Inhibitory mechanism of mimosa tannin using molecular modeling and substitutional adsorption isotherms, Mater. Chem. Phys. 77 (2003) 97–102.
[28] Z. Cao, Y. Tang, H. Cang, J. Xu, G. Lu, W. Jing, Novel benzimidazole derivatives as corrosion inhibitors of mild steel in the acidic media. Part II: Theoretical studies, Corros. Sci. 83 (2014) 292–298.
[29] A. Kokalj, On the HSAB based estimate of charge transfer between adsorbates and metal surfaces, Chem. Phys. 393 (2012) 1–12.
[30] W. Yang, W.J. Mortier, The use of global and local molecular parameters for the analysis of the gas-phase basicity of amines, J. Am. Chem. Soc. 108 (1986) 5708–5711, https://doi.org/10.1021/ja00279a008.
[31] C. Morell, A. Grand, A. Toro-Labbe, New dual descriptor for chemical reactivity, J. Phys. Chem. A 109 (2005) 205–212.
[32] H. Mi, G. Xiao, X. Chen, Theoretical evaluation of corrosion inhibition performance of three antipyrine compounds, Comput. Theor. Chem. 1072 (2015) 7–14, https://doi.org/10.1016/j.comptc.2015.08.023.
[33] L. Guo, I.B. Obot, X. Zheng, X. Shen, Y. Qiang, S. Kaya, C. Kaya, Theoretical insight into an empirical rule about organic corrosion inhibitors containing nitrogen, oxygen, and sulfur atoms, Appl. Surf. Sci. 406 (2017) 301–306, https://doi.org/10.1016/j.apsusc.2017.02.134.
[34] H. Hu, X. Li, Z. Fang, N. Wei, Q. Li, Small-molecule gas sorption and diffusion in coal: molecular simulation, Energy 35 (2010) 2939–2944, https://doi.org/10.1016/j.energy.2010.03.028.
[35] H. Sun, COMPASS: an ab initio force-field optimized for condensed-phase applications overview with details on alkane and benzene compounds, J. Phys. Chem. B 102 (1998) 7338–7364, https://doi.org/10.1021/jp980939v.
[36] H.C. Andersen, Molecular dynamics simulations at constant pressure and/or temperature, J. Chem. Phys. 72 (1980) 2384–2393, https://doi.org/10.1063/1.439486.
[37] J. Haque, V. Srivastava, C. Verma, H. Lgaz, R. Salghi, M.A. Quraishi, N -Methyl- N, N, N -trioctylammonium chloride as a novel and green corrosion inhibitor for mild steel in an acid chloride medium: Electrochemical, DFT and MD studies, New J. Chem. 41 (2017) 13647–13662, https://doi.org/10.1039/c7nj02254a.
[38] A.V. Shanbhag, T.V. Venkatesha, R.A. Prabhu, B.M. Praveen, Inhibition effects of acetyl coumarines and thiazole derivatives on corrosion of zinc in acidic medium, Bull. Mater. Sci. 34 (2011) 571–576.
[39] I.H.R. Tomi, A.H.R. Al-Daraji, S.A. Aziz, Synthesis, Characterization, and Study the Inhibitory Effect of Thiazole and Thiadiazole Derivatives toward the Corrosion of Copper in Acidic Media, Synth. React. Inorg. Met. 45 (2015) 605–613, https://doi.org/10.1080/15533174.2013.841226.
[40] K.F. Khaled, M.A. Amin, Corrosion monitoring of mild steel in sulphuric acid solutions in presence of some thiazole derivatives – molecular dynamics, chemical and electrochemical studies, Corros. Sci. 51 (2009) 1964–1975, https://doi.org/10.1016/j.corsci.2009.05.023.
[41] A.E. Fouda, A. Al-Sarawy, E. Elkatori, Thiazole derivatives as corrosion inhibitors for C-steel in sulphuric acidsolution, Eur. J. Chem. 1 (2010) 312–318, https://doi.org/10.5155/eurjchem.1.4.312-318.105.
[42] A.K. Singh, S. Mohapatra, B. Pani, Corrosion inhibition effect of Aloe Vera gel: gravimetric and electrochemical study, J. Ind. Eng. Chem. 33 (2016) 288–297, https://doi.org/10.1016/j.jiec.2015.10.014.
[43] A.K. Singh, M.A. Quraishi, The effect of some bis-thiadiazole derivatives on the corrosion of mild steel in hydrochloric acid, Corros. Sci. 52 (2010) 1373–1385, https://doi.org/10.1016/j.corsci.2010.01.007.
[44] O.L. Riggs Jr., R.M. Hurd, Temperature coefficient of corrosion inhibition, Corrosion 23 (1967) 252–260, https://doi.org/10.5006/0010-9312-23.8.252.
[45] E.A. Noor, A.H. Al-Moubaraki, Thermodynamic study of metal corrosion and inhibitor adsorption processes in mild steel/1-methyl-4[4′(-X)-styryl pyridinium iodides/hydrochloric acid systems, Mater. Chem. Phys. 110 (2008) 145–154, https://doi.org/10.1016/j.matchemphys.2008.01.028.
[46] A. Yurt, A. Balaban, S.U. Kandemir, G. Bereket, B. Erk, Investigation on some Schiff bases as HCl corrosion inhibitors for carbon steel, Mater. Chem. Phys. 85 (2004) 420–426, https://doi.org/10.1016/j.matchemphys.2004.01.033.
[47] P. Liu, B. Garrido, K. Oksman, A.P. Mathew, Adsorption isotherms and mechanisms of Cu (II) sorption onto TEMPO-mediated oxidized cellulose nanofibres, RSC Adv. 6 (2016) 107759–107767, https://doi.org/10.1039/C6RA22397D.
[48] C. Yi, B. Zhu, Y. Chen, X. Du, Y. Yang, J. Liu, Z. Zhang, Adsorption and protective behaviour of BTAH on the initial atmospheric corrosion process of copper under thin film of chloride solutions, Sci. Rep. 8 (2018) 5606, https://doi.org/10.1038/s41598-018-23927-w.
[49] A.F.S.A. Rahiman, S. Sethumanickam, Corrosion inhibition, adsorption and thermodynamic properties of ploy(vinyl alcohol-cysteine)in molar HCl, Arab. J. Chem. 10 (2017) S3358–S3366, https://doi.org/10.1016/j.arabjc.2014.01.016.
[50] N.A. Negm, M.F. Zaki, Corrosion inhibition efficiency of nonionic Schiff base amphiphiles of p-amino benzoic acid for aluminium in 4 N HCl, Colloid Surf. A Physiochem. Eng. Aspec. 322 (2008) 97–102, https://doi.org/10.1016/j.colsurfa.2008.02.027.
[51] A.K. Singh, M.A. Quraishi, Effect of 2, 2'benzothiazolyl disulfide on the corrosion of mild steel in acid media, Corros. Sci. 51 (2009) 2752–2760, https://doi.org/10.1016/jcorsci.2009.07.011.
[52] M.T. Amin, A.A. Alazba, M. Shafiq, Adsorptive removal of reactive black 5 from wastewater using bentonite clay: isotherms, kinetics and thermodynamics, Sustain 7 (2015) 15302–15318, https://doi.org/10.3390/su71115302.
[53] B. Chugh, A.K. Singh, S. Thakur, B. Pani, A.K. Pandey, H. Lgaz, I.M. Chung, E.E. Ebenso, An exploration about the interaction of mild steel with hydrochloric acid in the presence of N-(Benzo[d]thiazole-2-yl)-1-phenylethan-1-imines, J. Phys. Chem. C123 (2019) 22897–22917, https://doi.org/10.1021/acs.jpcc.9b03994.
[54] M.E. Faydy, R. Touir, M.E. Touhami, A. Zarrouk, C. Jama, B. Lakhrissi, L.O. Olasunkanmi, E.E. Ebenso, F. Bentiss, Corrosion inhibition performance of newly synthesized 5-alkoxymethyl-8-hydroxyquinoline derivatives for carbon steel in 1 M HCl solution: experimental, DFT and Monte Carlo simulation studies, Phys. Chem. Chem. Phys. 20 (2018) 20167–20187, https://doi.org/10.1039/C8CP03226B.
[55] B. Ramezanzadeh, S.Y. Arman, M. Mehdipour, B.P. Markhali, Analysis of electrochemical noise (ECN) data in time and frequency domain for comparison corrosion inhibition of some azole compounds on Cu in 1.0 M H2SO4 solution, Appl. Surf. Sci. 289 (2014) 129–140, https://doi.org/10.1016/j.apsusc.2013.10.119.
[56] L. Feng, C. Yin, H. Zhang, Y. Li, X. Song, Q. Chen, H. Liu, Cationic gemini surfactants with a bipyridyl spacer as corrosion inhibitors for carbon steel, ACS Omega 3 (2018) 18990–18999, https://doi.org/10.1021/acsomega.8b03043.
[57] A.K. Singh, Inhibition of mild steel corrosion in hydrochloric acid solution by 3-(4-((Z)-indolin-3-ylideneamino) phenylimino) indolin-2-one, Ind. Eng. Chem. Res. 51 (2012) 3215–3223, https://doi.org/10.1021/ie2020476.
[58] A.S. Fouda, M. Eissa, G.Y. Elewady, W.T. El, Corrosion inhibition of low carbon steel in 1 M HCl solution using Pulicaria undulata plant extract, Int. J. Electrochem. Sci. 12 (2017) 9212–9230.
[59] M. Yadav, R.R. Sinha, S. Kumar, T.K. Sarkar, Corrosion inhibition effect of spiro pyrimidine thiones on mild steel in 15% HCl solution insight from: electrochemical and quantum studies, RSC Adv. 5 (2015) 70832–70848, https://doi.org/10.1039/C5RA14406J.
[60] H. Lgaz, I.-M. Chung, R. Salghi, I.H. Ali, A. Chaouiki, Y. El Aoufir, M.I. Khan, On the understanding of the adsorption of Fenugreek gum on mild steel in an acidic medium: insights from experimental and computational studies, Appl. Surf. Sci. 463 (2019) 647–658, https://doi.org/10.1016/j.apsusc.2018.09.001.
[61] S. Pareek, D. Jain, S. Hussain, A. Biswas, R. Shrivastava, S.K. Parida, H.K. Kisan, H. Lgaz, I.-M. Chung, D. Behera, A new insight into corrosion inhibition mechanism of copper in aerated 3.5 wt. % NaCl solution by eco-friendly Imidazopyrimidine Dye: experimental and theoretical approach, Chem. Eng. J. 358 (2019) 725–742, https://doi.org/10.1016/j.cej.2018.08.079.
[62] A. Singh, K.R. Ansari, J. Haque, P. Dohare, H. Lgaz, R. Salghi, M.A. Quraishi, Effect of electron donating functional groups on corrosion inhibition of mild steel in hydrochloric acid: experimental and quantum chemical study, J. Taiwan Inst. Chem. Eng. 82 (2018) 233–251, https://doi.org/10.1016/j.jtice.2017.09.021.
[63] R. Kumar, S. Chahal, S. Kumar, S. Lata, H. Lgaz, R. Salghi, S. Jodeh, Corrosion inhibition performance of chromone-3-acrylic acid derivatives for low alloy steel with theoretical modeling and experimental aspects, J. Mol. Liq. 243 (2017) 439–450, https://doi.org/10.1016/j.molliq.2017.08.04.
[64] K.F. Khaled, Experimental, density function theory calculations and molecular dynamics simulations to investigate the adsorption of some thiourea derivatives on iron surface in nitric acid solutions, Appl. Surf. Sci. 256 (2010) 6753–6763, https://doi.org/10.1016/j.apsusc.2010.04.085.
[65] A. Chaouiki, H. Lgaz, I.M. Chung, I.H. Ali, S.L. Gaonkar, K.S. Bhat, R. Salghi, H. Oudda, M.I. Khan, Understanding corrosion inhibition of mild steel in acid medium by new benzonitriles: insights from experimental and computational studies, J. Mol. Liq. 266 (2018) 603–616, https://doi.org/10.1016/j.molliq.2018.06.103.
[66] A. Singh, K.R. Ansari, M.A. Quraishi, H. Lgaz, Y. Lin, Synthesis and investigation of pyran derivatives as acidizing corrosion inhibitors for N80 steel in hydrochloric acid: theoretical and experimental approaches, J. Alloys. Compd. 762 (2018) 347–362, https://doi.org/10.1016/j.jallcom.2018.05.236.
[67] C. Verma, H. Lgaz, D.K. Verma, E.E. Ebenso, I. Bahadur, M.A. Quraishi, Molecular dynamics and Monte Carlo simulations as powerful tools for study of interfacial adsorption behavior of corrosion inhibitors in aqueous phase: a review, J. Mol. Liq. 260 (2018) 99–120, https://doi.org/10.1016/j.molliq.2018.03.045.
[68] I.B. Obot, K. Haruna, T.A. Saleh, Atomistic simulation: a unique and powerful computational tool for corrosion inhibition research, Arab. J. Sci. Eng. 44 (2019) 1–32, https://doi.org/10.1007/s13369-018-3605-4.
[69] A. Dutta, S.K. Saha, P. Banerjee, D. Sukul, Correlating electronic structure with corrosion inhibition potentiality of some bis-benzimidazole derivatives for mild steel in hydrochloric acid: combined experimental and theoretical studies, Corros. Sci. 98 (2015) 541–550, https://doi.org/10.1016/j.corsci.2015.05.065.
[70] H. Shokry, M. Yuasa, I. Sekine, R.M. Issa, H.Y. El-Baradie, G.K. Gomma, Corrosion inhibition of mild steel by Schiff ; base compounds in various aqueous solutions: part 1, Corros. Sci. 40 (1998) 2173–2186, https://doi.org/10.1016/S0010-938X(98)00102-4.
[71] S. John, B. Joseph, K.V. Balakrishnan, K.K. Aravindakshan, A. Joseph, Electrochemical and quantum chemical study of 4-[(E)-[(2,4-dihydroxy phenyl) methylidine] amino]-6-methyl-3-sulphanylidine-2,3,4,5-tetra hydro-1,2,4-triazin-5-one [DMSTT], Mater. Chem. Phys. 123 (2010) 218–224, https://doi.org/10.1016/j.matchemphys.2010.03.085.
[72] X. Luo, C. Ci, J. Li, K. Lin, S. Du, H. Zhang, X. Li, Y.F. Cheng, J. Zang, Y. Liu, 4-Aminoazobenzene modified natural glucomannan as a green eco-friendly inhibitor for the mild steel in 0.5 m HCl solution, Corros. Sci. 151 (2019) 132–142.